5.4.1 x-direction wind

Figure 5.13 gives the overall heat transfer for units 1, 2 and 3 of the Large ACSC subject to a positive x-direction wind and also the contribution of fan performance and plume recirculation on the ACSC effectiveness respectively.

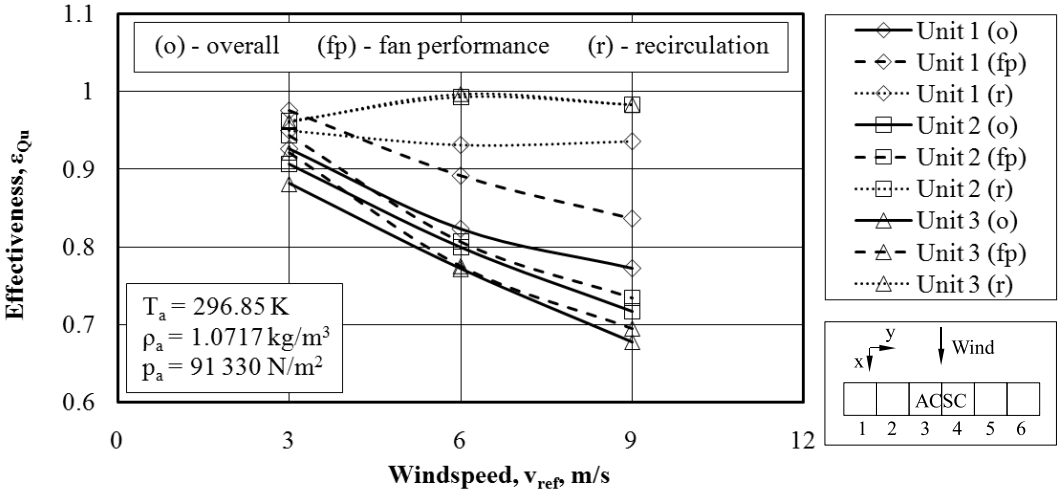

Figure 5.13: Illustration of the overall effectiveness as a result of the contribution of fan performance and plume recirculation for a positive x-direction wind

It is seen that for the case of a 3 m/s wind, the recirculation at unit 1 is the main contributor to the performance reduction. In addition, recirculation increases at unit 1 with an increase in wind speed, but poor fan performance becomes the major contributor to the reduction in ACSC operation. Nevertheless the effect of recirculation is still significant at unit 1. Figure 5.13 also shows that plume recirculation reduces for units 2 and 3 as the wind speed approaches 6 m/s, but then increase again due to back flow occurring through some fans in row 1 of the ACSC. Regardless of this, the contribution of poor fan performance outweighs the effect of recirculation for the overall effectiveness of units 2 and 3.

5.4.2 y-direction wind

An illustration of the contribution of fan performance and recirculation on the overall effectiveness of the Large ACSC subject to a positive y-direction wind is shown in figure 5.14 for all the cooling units in the ACSC.

Fan performance is the main contributor to the reduction in ACSC operation, but from the results obtained, only unit 1 shows a significant decrease in effectiveness. Furthermore a reduction in the effectiveness of unit 2 is only

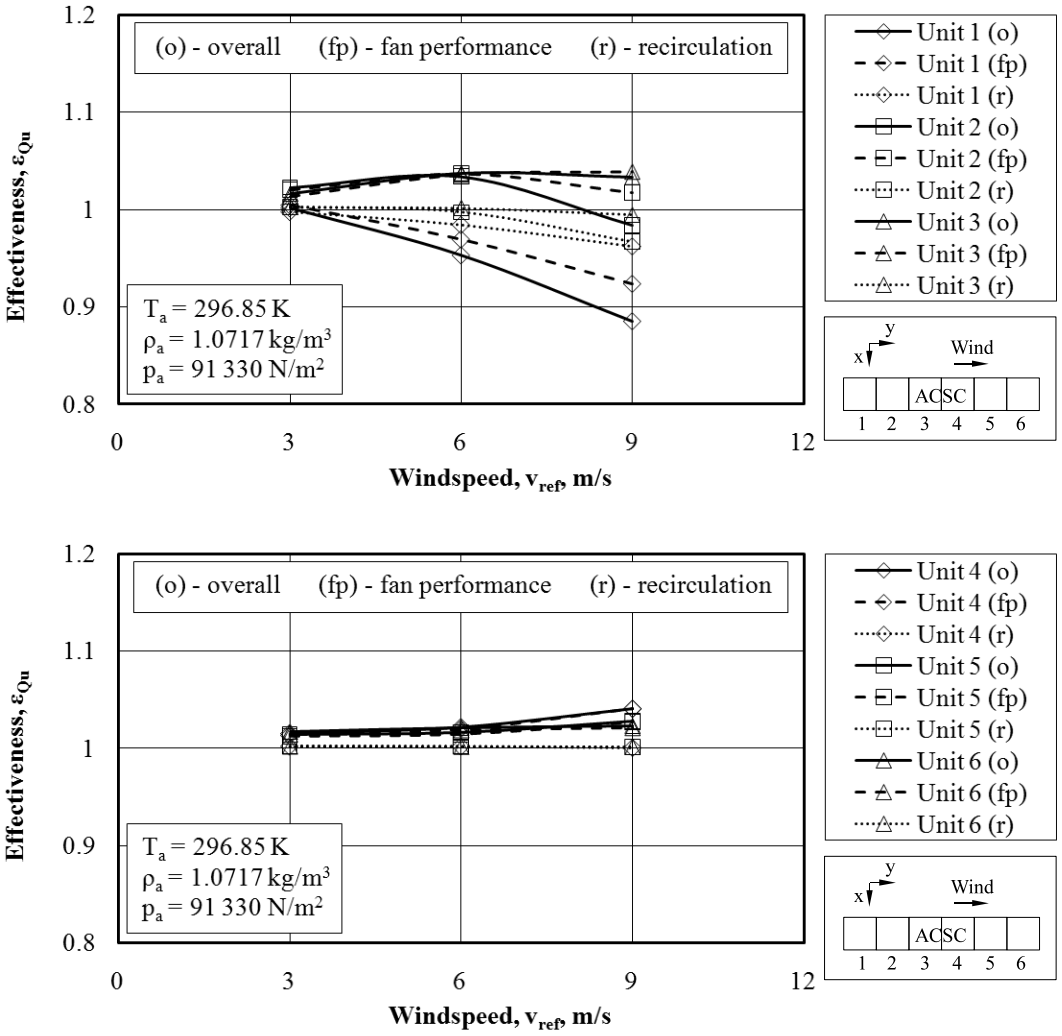

Figure 5.14: Illustration of the overall effectiveness as a result of the contribution of fan performance and plume recirculation for a positive y-direction wind

seen at 9 m/s, mainly due to recirculation.

In contrast to this, the effectiveness of the other downstream units (3-6) increase beyond 100 % and recirculation has little or no effect on the overall cooling performance of the units. From figure 5.14 it could be assumed that the fans situated in the ACSC (especially further downstream of the leading periphery) have the ability to exploit the energy in the wind to a certain extent, therefore drawing in more flow compared to ideal flow. This was also noticed by Van Rooyen (2007), Owen (2010) and Joubert (2010) as the fans placed the furthest downstream in their respective ACSC's showed a volumetric flow rate of more than 100 %. The ACSC's in their research however only extended to five rows and as a consequence the trend seen in the present study was not observed.

5.4.3 Conclusion

The results obtained for both wind directions show that fan performance predominantly affects the effectiveness of the free standing Large ACSC. However it must be noted that reduced fan performance is far more severe for the case of x-direction winds compared to y-direction winds. Furthermore, plume recirculation is also worse for the former wind condition, compared to the latter.

In practice, ACSC's are built so that the long side is situated perpendicular to the predominant wind direction (in this case the x-direction). However this exposes far more fans to the separation occurring on this periphery compared to the number of exposed fans for y-direction winds. Moreover, separation is worse for x-direction winds than y-direction winds due to effects such as two-dimensional and cross-flow as well as the higher elevation from which air is drawn into the ACSC.

It seems that it might be possible to obtain a very large improvement, regarding the elimination of poor fan performance and plume recirculation, if the ACSC was constructed such that the predominant wind direction flows parallel to the length of the ACSC. In practice however, buildings are located in the vicinity of the ACSC and therefore an investigation into the influence of buildings on ACSC performance would be interesting. Furthermore wind directions are unconstrained and therefore some wind mitigation measures need to be implemented to ensure an improved overall ACSC performance during these windy periods. The investigation of the effect of these measures on the Large ACSC is discussed in chapter 6

5.5 Effect of main power plant buildings

The effect of the main power plant buildings (boiler houses, auxiliary bays and turbine hall) on the effectiveness of the Large ACSC under wind, were investigated. Due to a limit in computational capacity, this was only done for a positive and negative x-direction wind, since symmetry could be used in these cases

5.5.1 Positive x-direction wind

The overall effectiveness of cooling units 1, 2 and 3 is given in figure 5.15 for positive x-direction winds, illustrating the effect of the power plant buildings on the ACSC effectiveness, compared to the freestanding ACSC effectiveness.

The effectiveness of all the units in the ACSC is improved with the power plant buildings in place. This was expected since the building provides a barrier for the wind, forcing more air upwards into the ACSC. Once again a

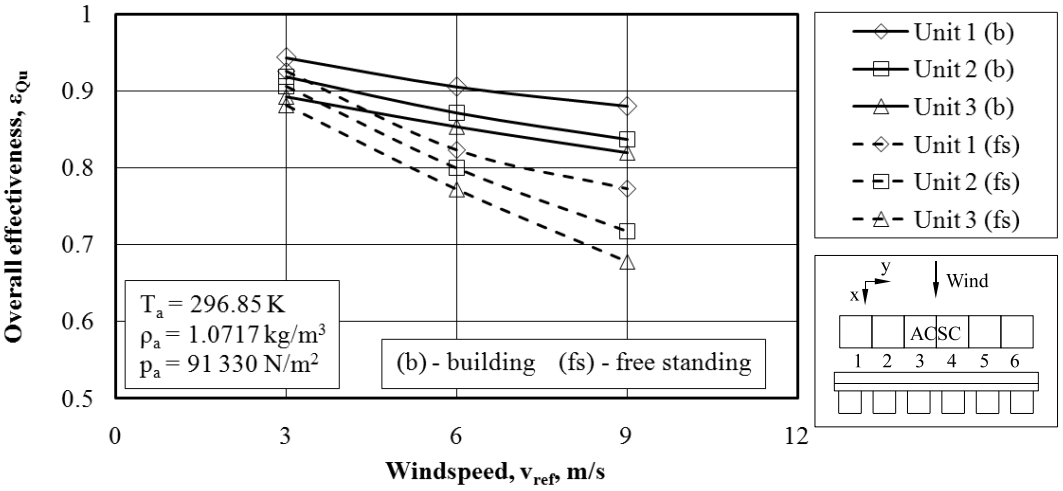

Figure 5.15: The overall effectiveness of units 1, 2 and 3, illustrating the effect of the main surrounding power station buildings during positive x-direction winds

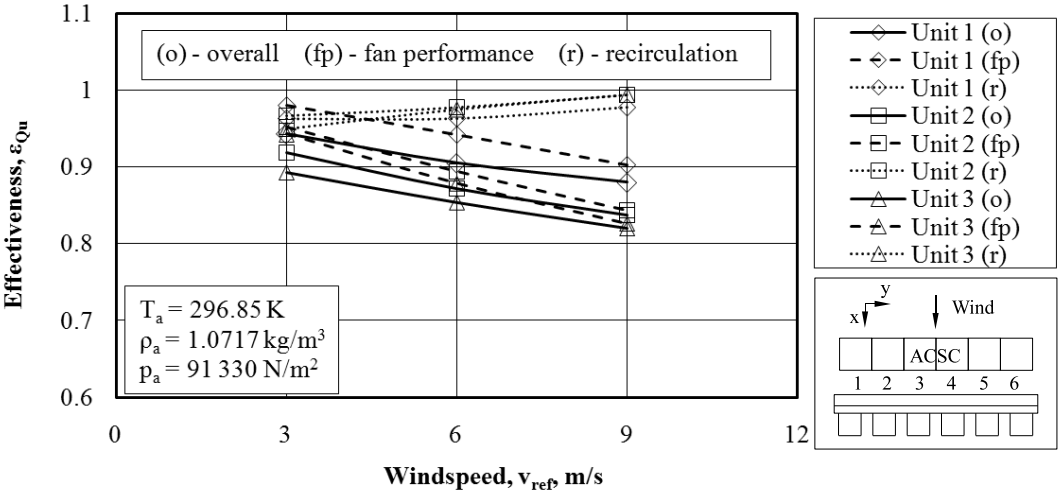

Figure 5.16: The overall effectiveness of units 1, 2 and 3, comparing the component of fan performance and plume recirculation on overall ACSC effectiveness during positive x-direction winds

decrease in ACSC effectiveness is seen for an increase in wind speed, but the gradient is smaller with the power station buildings in place compared to the case of a free standing ACSC.

A comparison between the individual effect of fan performance and plume recirculation can be seen in figure 5.16 for a positive x-direction wind. It shows that fan performance is the main contributor to the overall ACSC reduction, mainly due to the separation occurring on the upstream periphery.

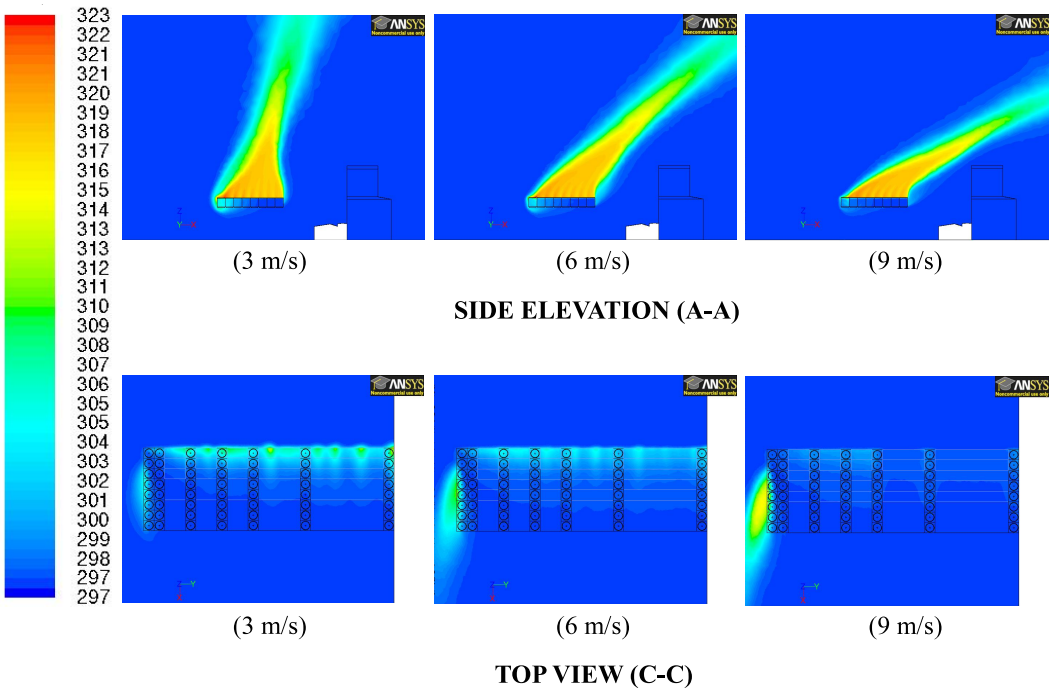

Figure 5.17: Contour plots of temperature, K, on planes A-A and B-B respectively for a 3 m/s, 6 m/s and 9 m/s positive x-direction wind

Plume recirculation decreases with an increase in wind speed as depicted by the contour plots in figure 5.17. This occurs since the region beneath the fan platform experiences an increase in pressure, with a progressive increase in positive x-direction wind speed, due to the proximity of the building. The increase in pressure beneath the platform provides more resistance to recirculating flow from the top of the ACSC.

5.5.2 Negative x-direction wind

Gao *et al.* (2009) simulated an ACSC composed of 32 fans and found that plume recirculation was the main contributor to the performance reduction

of the ACSC when the approaching winds came from behind the main power station buildings relative to the position of the ACSC. Adverse recirculation into the ACSC was also confirmed by Goldschagg (1993) and Liu *et al.* (2009) for the same wind direction.

The effect of negative x-direction winds were therefore also simulated to verify if the placement of the building between the ACSC and the approaching wind would indeed make plume recirculation the primary contributor to loss in overall ACSC performance. The overall effectiveness of units 1, 2 and 3 is illustrated in figure 5.18. It can be seen that the overall ACSC performance decreases with an increase in wind speed up to 6 m/s. The effectiveness of units 1 and 2 increases with an increase in wind speed from 6 to 9 m/s, but the effectiveness of unit 3 decreases further.

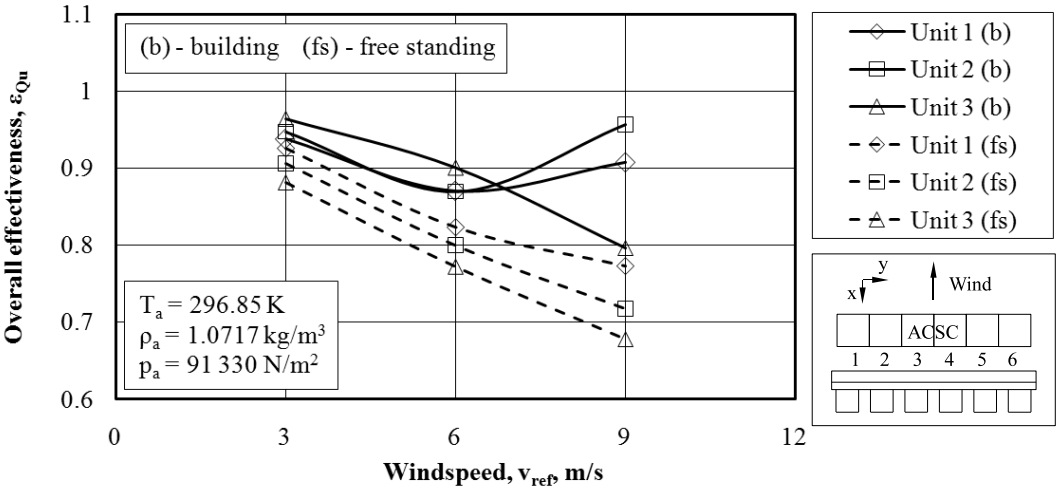

Figure 5.18: The overall effectiveness of units 1, 2 and 3, illustrating the effect of the main surrounding power station buildings during negative x-direction winds

Figure 5.19 shows the individual effects of fan performance and plume recirculation on the overall performance of ACSC for a negative x-direction wind. It shows that the plume recirculation is generally the main contributor to the reduction in ACSC performance. This can be seen by the contour plot in figure 5.20. Large amounts of plume air are recirculated beneath the fan platform at the upstream periphery especially for unit 3, therefore explaining the decrease in effectiveness for a 9 m/s wind.

Arguably, the work of Gao *et al.* (2009) is verified, since it was shown that plume recirculation is the main contributor to reduced ACSC performance for the case of wind blowing from the back of the power plant buildings. The simulation of this wind direction is in actual fact not entirely symmetrical due

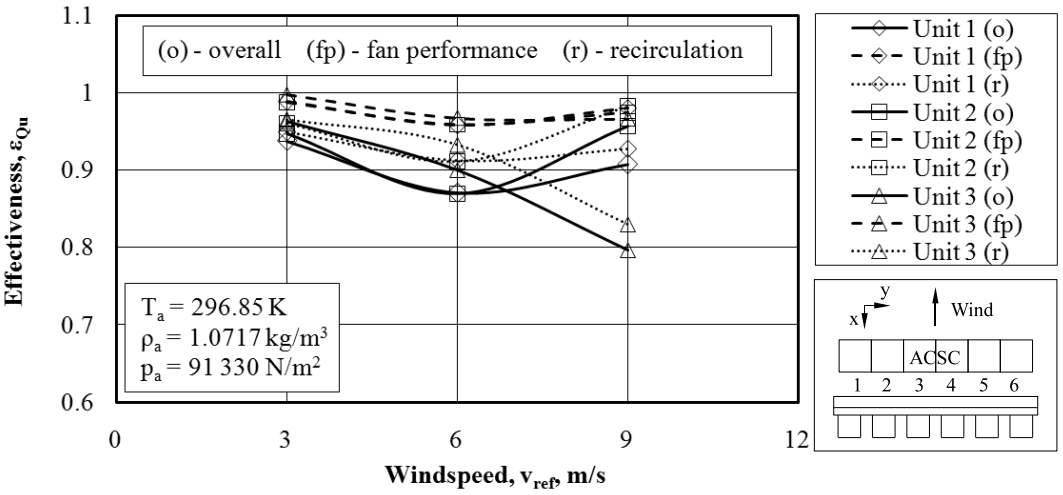

Figure 5.19: The overall effectiveness of units 1, 2 and 3, comparing the effect of fan performance and plume recirculation on overall ACSC effectiveness during negative x-direction winds

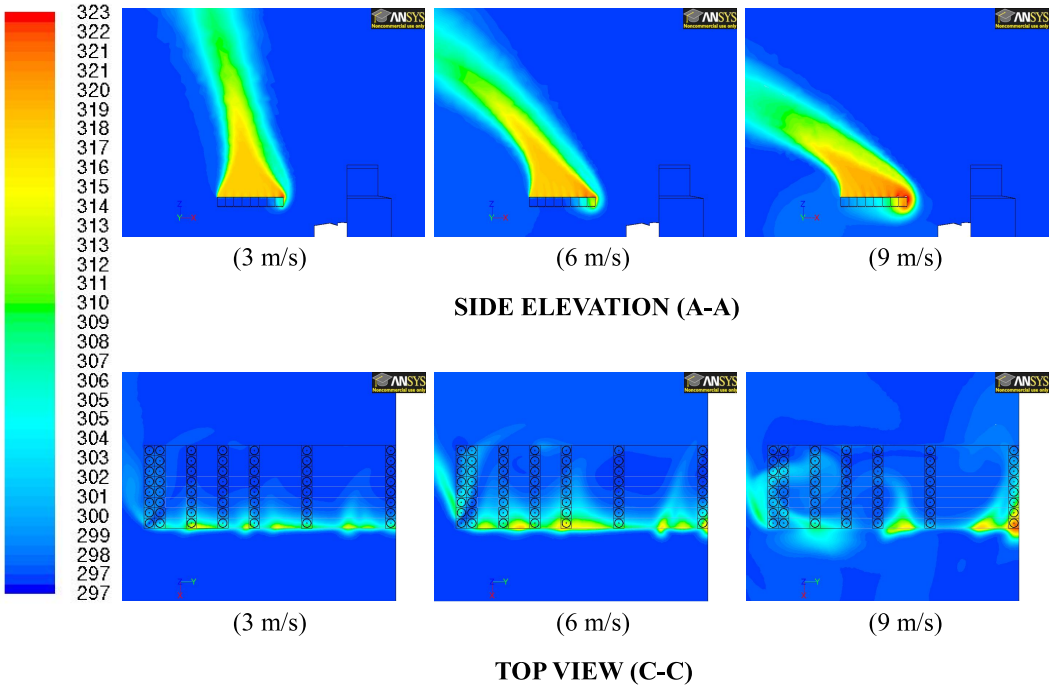

Figure 5.20: Contour plots of temperature, K, on planes A-A and B-B respectively for a 3 m/s, 6 m/s and 9 m/s negative x-direction wind

to the shape of the boiler houses. The x-direction wind analysis for the ACSC, with the placement buildings, does however give a realistic trend.

Chapter 6

Evaluation of ACSC wind mitigation modifications

The overall effectiveness of an ACSC could be improved by the addition of skirts along the periphery of and screens below the ACSC (seen in figure 6.1), as obtained by previous researchers (Duvenhage *et al.*, 1995), (Salta and Kröger, 1995), (Bredell, 2005), (Van Rooyen, 2007), (Owen, 2010) and (Joubert, 2010). Different variations of skirts and screens, implemented on the Large ACSC, were investigated in order to determine its effect on overall ACSC performance.

The effect of skirts and screens were investigated separately for a series of x-direction winds on the performance of a freestanding ACSC. Consequently, after these individual effects were known, only the combined effect of selected skirts and screens were investigated further for the following cases:

Case 1: Positive x-direction winds on a freestanding ACSC

Case 2: Positive y-direction winds on a freestanding ACSC

Case 3: Positive and negative x-direction winds on the ACSC, taking the proximity of the power station buildings into account

6.1 Effect of skirts

Different skirt widths were investigated to compare their individual influence on the performance of the Large ACSC. Additionally the change in Large ACSC effectiveness due to an *elliptic* skirt was also investigated. The two different skirt configurations and their dimensions are shown in figure 6.2 and labeled as shown in table 6.1:

The addition of a skirt to the periphery of the ACSC, shifts the region of separation (seen in figure 5.3) further upstream of the edge fans. Through this

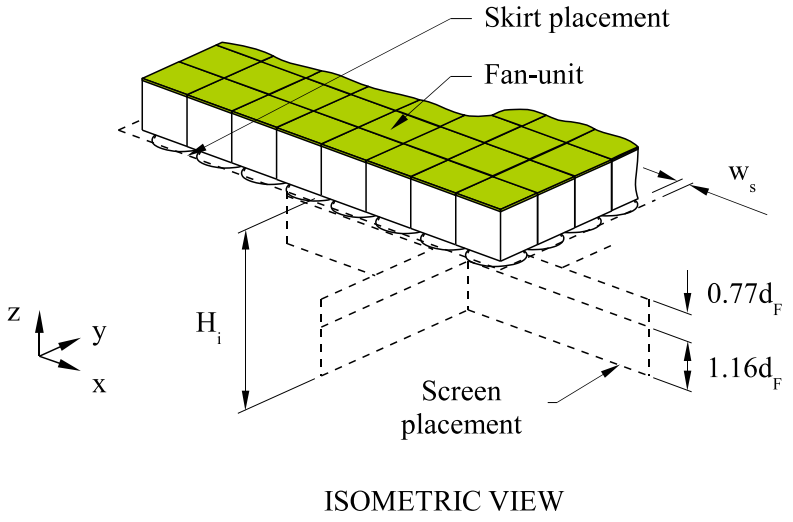

Figure 6.1: Skirt and screen placements along the periphery of and beneath the Large ACSC

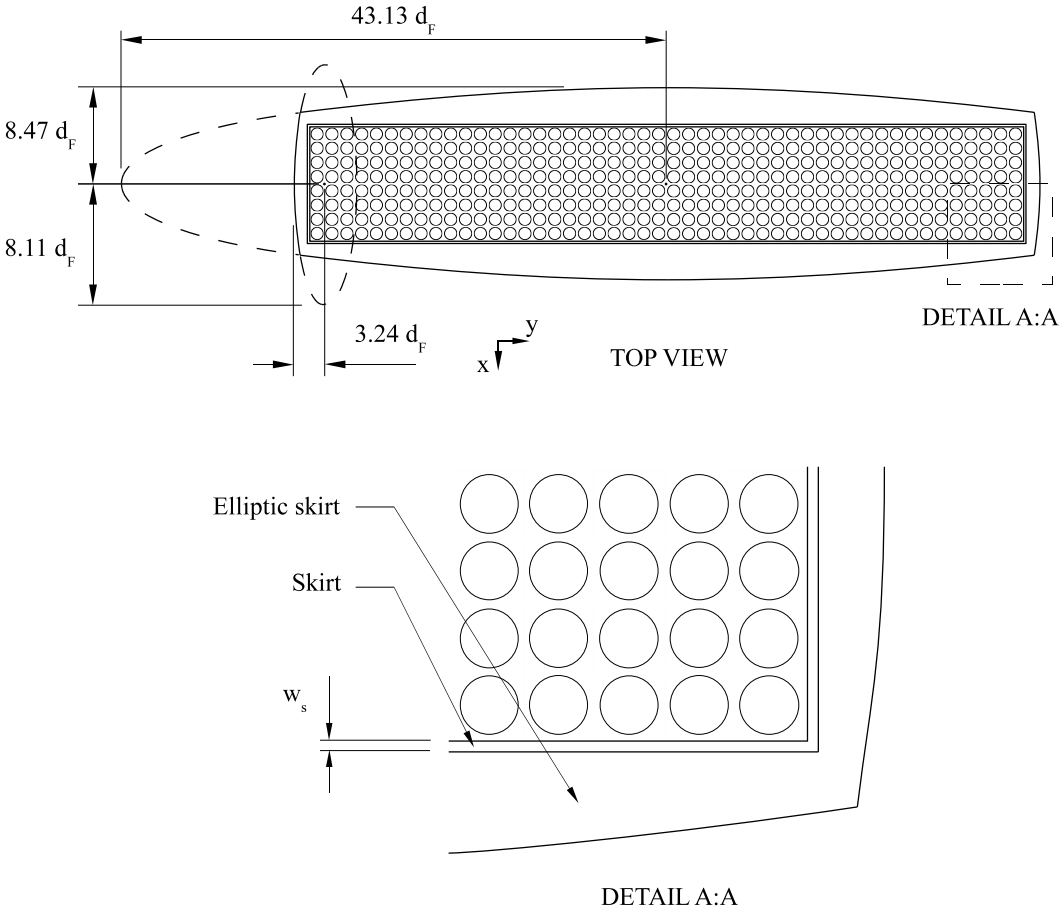

Figure 6.2: Different skirt placements along the periphery of the Large ACSC

Table 6.1: Skirt labels

Skirt label	Specification, m
sk 1	$w_s = 0.241 d_F$
sk 2	$w_s = 0.482 d_F$
sk 3	$w_s = 0.724 d_F$
sk 4	*elliptic* (figure 6.2)

modification, an attempt was made to improve the flow through the upstream fans and consequently improve the overall effectiveness of the Large ACSC. This is however not always the case as can be seen by the overall effectiveness, plotted in figure F.1 (a), (b) and (c) of appendix F, for units 1, 2 and 3 respectively.

Figure F.1 shows that the overall effectiveness of each cooling unit is progressively improved for an increase in skirt width, except for skirt *sk 1* in the case of units 2 and 3. The performance of unit 2 remains approximately unchanged with the addition of *sk 1*, whereas the performance of unit 3 is reduced. The reduced ACSC performance in these cases are due to a significant reduction in flow through certain fans in the second row (shown in figure 6.3 for a 6 m/s positive x-direction wind) with the implementation of skirt *sk 1*.

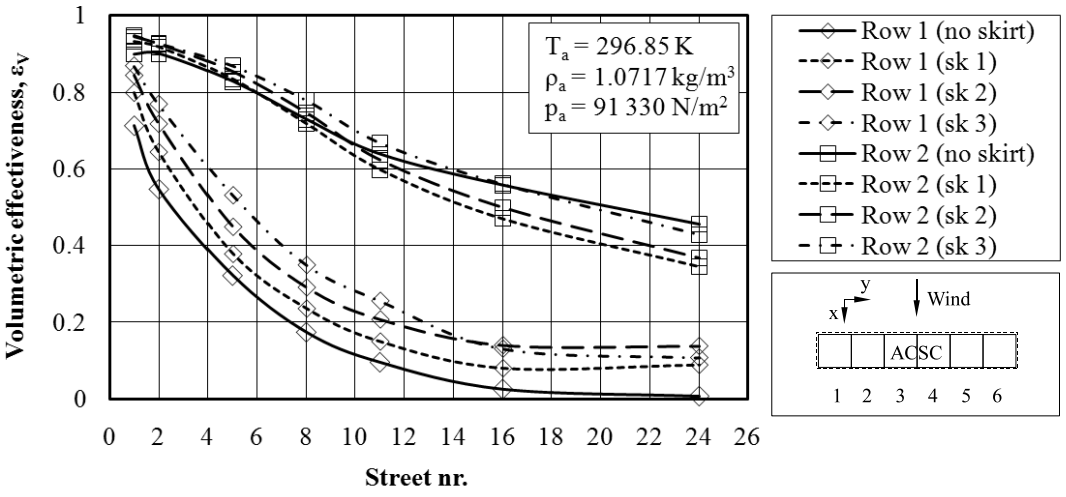

Figure 6.3: The effect of various skirts on the volumetric effectiveness of rows 1 and 2 for a positive x-direction wind of 6 m/s

The reason for the reduction in flow through some fans in the second row is

not entirely clear. The pressure contour plots, illustrated in figure 5.3, shows that the separation occurring at the upstream periphery, closer to the symmetry plane of the ACSC, extends across more than two fan rows (downwind). Skirt *sk 1* displaces the separated flow with a margin of $0.241d_F$ m upstream from the periphery fans, which is only a fraction of one fan diameter. Consequently the fans in the upstream rows of cooling units 2 and 3 are still subject to severe distorted flow. This distorted flow might alter the flow at the upstream periphery, in the two-dimensional flow region, to such an extent that the flow through the fan in row 1 is improved, but reduces the fan performance of row 2.

From figure 5.3 it can be seen that the region of separation below the ACSC is partially formed in the shape of an ellipse and that it grows larger with an increase in wind speed. In an attempt to counter this separation region, a skirt was investigated with a similar elliptical shape, in effect mirroring the shape of the separation occurring for a 9 m/s x-direction wind. This wind speed was chosen since the skirt size would effectively counter the separated region for all wind speeds lower than 9 m/s, if it counters the separation region for a 9 m/s wind. This skirt shape showed a significant increase in flow through the ACSC compared to the *ordinary* skirts.

In conclusion the following should be noted:

- The addition of a skirt to the Large ACSC progressively improved the flow through unit 1, with an increase in skirt width, since the skirt width of *sk 1* and larger, seems to effectively move the separation region away from most of the upstream fans. The skirt width however becomes less effective towards units 2 and 3 of the Large ACSC, since the separated region extends across a width, considerably greater than that of skirts *sk 1*, *2* and *3*.
- The addition of an *elliptical* skirt significantly improves the flow though all the cooling units of the Large ACSC, since the width of the skirt progressively increases towards cooling units 2 and 3, similar to the width of the separated flow region beneath the ACSC platform. As a consequence the separation region shifts upstream from the periphery of the ACSC, proportional to the changing skirt width, improving the flow through the Large ACSC.

6.2 Effect of screens and deflection walls

The influence of various screens on the overall performance of the ACSC was also investigated. The screen configuration, shown in figure 6.4 (a), is divided

into two levels. Level 1 (closest to the ground) has a zero porosity, whereas level 2 is porous. Different porosities for level 2 were modeled by specifying a loss coefficient, K_{l2}, for this part of the screen. Additionally the effect of a deflection wall, shown in figure 6.4 (b), on overall ACSC performance was also investigated. The various loss coefficients (for level 2 of the screen), their associated labels and the label for the deflection wall used in the present study, are given in table 6.2.

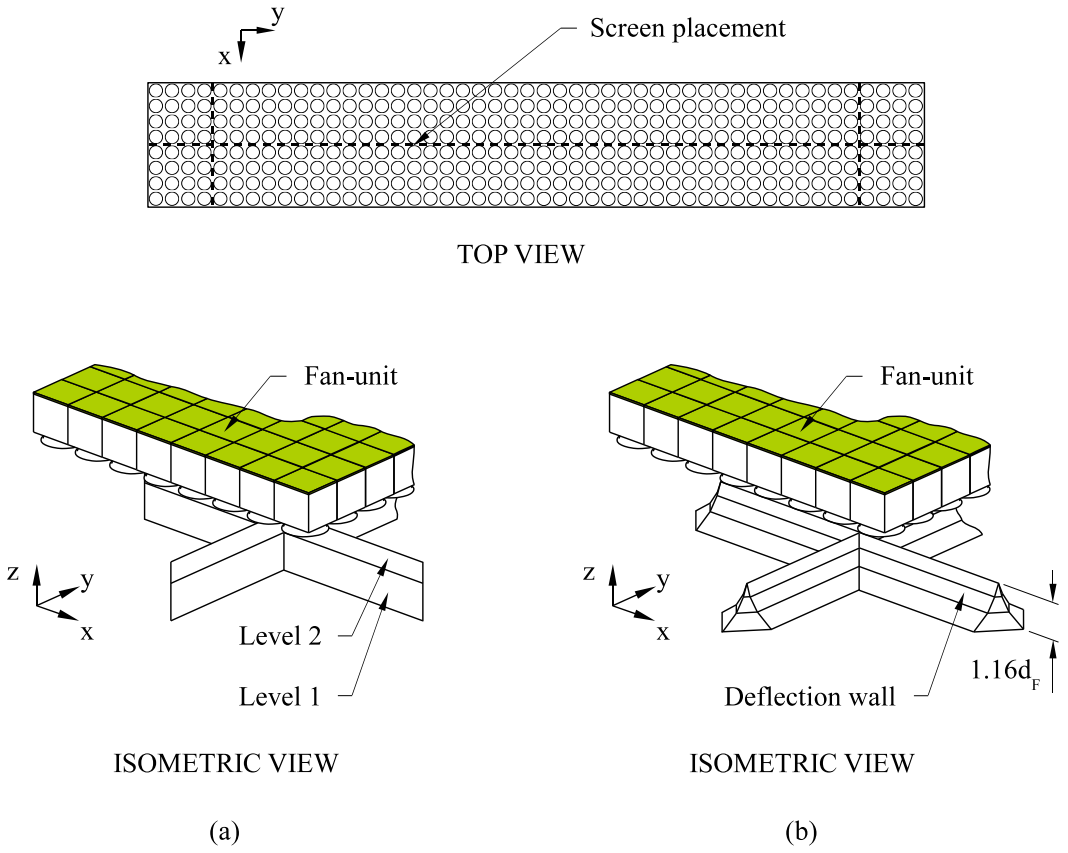

Figure 6.4: Placement of screens and the deflection wall beneath the Large ACSC

The effect of various screens and the deflection wall on the overall performance of the Large ACSC is shown in figure F.2 for the ACSC subject to x-direction winds. The performance results, due to the various screen configurations, show a measurable increase in overall effectiveness of the Large ACSC compared to the effect of skirts. For a 3 m/s wind speed the overall effectiveness of all three cooling units are close to 100 % and reduces slightly for higher wind speeds, but still remain within 5 % of a 100 % performance up to a wind speed of 9 m/s.

Table 6.2: Screen labels and corresponding loss coefficients of screen level 2

Screen label	K_{l2}
sc 1	0
sc 2	2.18
sc 3	5
sc 4	10
sc 5	∞
sc 6	*deflection wall*, ∞

The implementation of screens below the ACSC platform, effectively counters the through flow, seen in figure 5.4, from occurring. The region below the ACSC, experiences a rise in pressure (similar to the effect due to the power station buildings discussed previously) and consequently the approaching air is forced upwards into the ACSC. Due to the higher pressure beneath the ACSC platform, airflow is improved through the ACSC, which greatly reduces the separation region beneath the ACSC platform (seen in figure 6.5) on the upstream periphery as well as recirculation.

In conclusion the following should be noted:

- The ACSC effectiveness obtained due to the various screens in the present study is very similar.
- The vertical screen *sc 1* and the deflection wall (*sc 6*), having the same height, give similar performance results, despite the difference in geometry. These screens are also the least effective of all the screens analyzed.
- Screen *sc 5* proved to be the greatest improvement amongst the screens investigated, with screen level 2 having a loss coefficient of infinity, effectively similar to *sc 1* with an increased height.

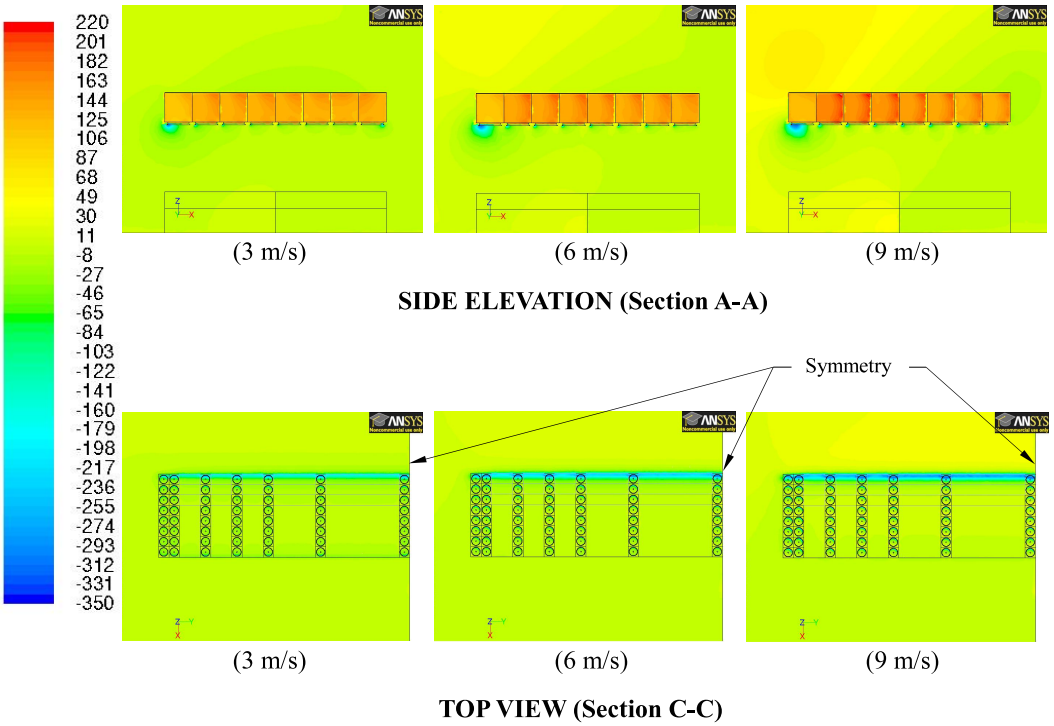

Figure 6.5: Contour plots of static pressure, N/m^2, on planes A-A and C-C respectively for the case of a 3 m/s, 6 m/s and 9 m/s positive x-direction and the implementation of screen *sc 2*

6.3 Combined effect of skirts and screens

The combined effect of certain skirts and screens were analyzed for the three cases stated previously and are discussed in the subsections hereafter. The combinations of skirts and screens are given in table 6.3:

Table 6.3: Different skirt-screen combinations that were evaluated

Combination	Skirt	Screen
1	sk 1	sc 2
2	sk 2	sc 4

6.3.1 Case 1

The effect of the skirt-screen combinations on the overall performance of the Large ACSC for positive x-direction winds were investigated. The overall ef-

fectiveness for this case is shown in figure F.3.

The results show a slight improvement from the case where only screens were investigated for the same wind direction. Implementing a skirt together with a screen improves the flow through the upstream fans even more since the separation occurring at the upstream periphery, though greatly reduced by the implemented screen, is shifted further upstream of the fans located in the upwind rows. The results also show that a further improvement of the ACSC effectiveness could be obtained by means of a larger skirt and denser screen (Combination 2).

6.3.2 Case 2

The effect of the same skirt-screen combinations (previous subsection) on the overall performance of the Large ACSC for positive y-direction winds were investigated. The overall effectiveness for this case is shown in figure F.4.

For this case, the effectiveness of unit 1 is improved considerably with the implementation of a skirt screen combination. Once again combination 2 proves to be more effective compared to combination 1, especially at high wind speeds.

A reduced performance is however seen for unit 2, compared to the performance of the ACSC with no screens and skirts implemented. The screen beneath the ACSC at unit 1 becomes an obstruction for the flow entering unit 2. Despite this reduction, a nett increase in performance can be seen between units 1 and 2. The implemented skirt-screen combination is therefore still advantageous.

Comparing the effect of skirt-screen combinations on the overall effectiveness of the remaining cooling units to a case where no skirts or screens are implemented, shows a negligible difference, except for unit 6. The effectiveness of unit 6 is reduced in the same manner by which the effectiveness of unit 2 is reduced, since the section of screen beneath unit 6 obstructs some of the flow from entering the fan-units located downwind of the screen placement.

6.3.3 Case 3

For case 3, the performance of the ACSC was investigated for a positive and negative x-direction wind, taking into account the mentioned skirt-screen combinations (previous two subsections) as well as the power station buildings. The overall effectiveness for the respective wind directions is shown in figures F.5 and F.5.

The overall effectiveness of the ACSC for a positive x-direction wind shows a significant increase for the implemented skirt-screen combinations for all cooling units in the ACSC compared to the case where no skirts or screens were implemented. The effectiveness is however slightly lower than the effectiveness of a freestanding ACSC with the same skirt-screen combination implemented. This is discussed to more detail in section 7.2. A similar improvement in ACSC effectiveness is seen for a negative x-direction wind.

Chapter 7

Conclusion

The goal of the present study was to design and build a simplified numerical model for the Large ACSC under investigation. Once the model was obtained and verified, simulations could be done in order to evaluate performance trends of the ACSC during windy conditions. Subsequently the effect of power station buildings and various wind mitigation measures were investigated in an attempt to improve the overall ACSC performance for steady windy conditions.

The performance results obtained for the free standing ACSC during positive x- and y-direction winds are discussed respectively. Consequently a discussion also follows regarding the effect of the various skirts, screens and the power station buildings for the applicable wind directions. The following conclusions can therefore be made regarding the present research.

7.1 Performance trends of the Large ACSC under wind

7.1.1 Positive x-direction wind

The reduction in performance of the ACSC under windy conditions is mainly due to reduced fan performance. For this case the contribution of fan performance is in the order of 2 to 30 %, where a 100 % effectiveness is defined as for ideal flow through every fan unit and no recirculation occuring. A decrease in fan performance is seen with an increase in wind speed, since the magnitude of separation occurring on the upstream periphery increase correspondingly. Furthermore it was noticed that flow approaching the ACSC progressively becomes two-dimensional, in the xz-plane, towards the symmetry plane of the ACSC. A greater magnitude of separation was observed on the upstream periphery in the two-dimensional flow region compared to the three-dimensional flow region. Inherently the fan performance of fans, close to the upstream periphery, experiencing two-dimensional flow, showed a greater decrease com-

pared to the fan performance on fans located in regions of the ACSC where the approaching flow is three-dimensional. The fans located in the last two rows (furthest downwind) interestingly showed an increase in performance to a value of more than 100 %, where 100 % refers to the case of ideal flow through a fan unit. This trend was also found by Van Rooyen (2007), Owen (2010) and Joubert (2010) showing that these fans have the ability to exploit the energy in the wind. It was observed that the performance of individual cooling units also reduced from units 1 to 3 as a result of the reduction in flow towards the symmetry plane of the ACSC.

Plume recirculation is observed around the upstream periphery of the ACSC as well as along the side parallel to the approaching wind. Recirculation on the upstream periphery also increases as the flow become more two-dimensional. This is mainly due to the entrainment of plume as the approaching air is progressively drawn from a higher elevation towards the symmetry plane of the ACSC compared to the air approaching the ACSC three-dimensionally further away from the symmetry plane. Recirculation along the open side, parallel to the wind direction, occurs due to vortex shedding of the flow in this region. This recirculation increases with a rise in wind speed since the vortex shedding intensifies. Plume recirculation along the side of the ACSC is generally greater compared to recirculation along the upstream periphery.

For this case it should be noted that the longest side of the ACSC is directly exposed to the approaching wind, consequently exposing a greater number of fans to the separation occurring on this edge during these winds, compared to y-direction winds. Even though reduced fan performance was the main contributor to a reduction in ACSC effectiveness, plume recirculation also contributed significantly and should not be neglected in the analysis of such a system.

7.1.2 Positive y-direction wind

The reduction in performance of unit 1 of the large ACSC for the y-direction was mainly due to a reduction in fan performance of the fans close to the upstream periphery. The reduction in ACSC effectiveness due to fan performance in this case is in the order of 0 to 10 % compared to a case where the flow through each fan unit is ideal. Units 2 and 3 both experience a slight reduction in ideal performance due to recirculation in the order of 0 to 4 %.

Interestingly, flow separation at the upstream periphery of the ACSC extends across a maximum of a single fan row for the y-direction wind, whereas separation extends across approximately three fan rows in the worst case of the x-direction wind. Separation, leading to a decrease in fan performance,

can therefore be reduced significantly if the ACSC is positioned such that the dominant wind approaches from the positive y-direction.

Moreover, a trend is observed (for the y-direction wind) where units 3 to 6 are all performing at an effectiveness between 100 % and 105 % for the range of wind speeds investigated in the present study. This is also observed for unit 2 up to a wind speed of $\approx$ 7.5 m/s. The increase in effectiveness is confirmed by the results obtained by Van Rooyen (2007), Owen (2010) and Joubert (2010) who also observed that the performance of the fans in the last row (downwind) of their respective ACSC's is higher than 100 %. It should also be noted that Van Rooyen (2007) observed this trend using the *actuator-disk* fan model, which is different to the *pressure-jump* fan method. If additional rows were added to the condenser of Van Rooyen (2007) (in the downwind direction), it could be expected that the performance of these fans would increase. Therefore it seems possible that the majority of the fans in the ACSC have the ability to exploit some of the energy in the wind and hence a performance effectiveness larger than 100 % could be obtained.

7.2 Effect of power station buildings and wind mitigation measures

7.2.1 Effect of power station buildings

The effect of power station building placement on the effectiveness of the ACSC was investigated for a positive and negative x-direction wind.

An improvement in the overall effectiveness of cooling units is observed for the positive x-direction wind, compared to the effectiveness of a free standing ACSC for the same wind. The region below the ACSC platform experiences a rise in pressure due to the obstruction of the building, forcing air into the ACSC. Reduced fan performance remains the main contributor to the performance reduction of the ACSC, except for cooling unit 1 during 3 m/s winds. The contribution of reduced fan performance ranges between 2 and 19 %. It is also noticed that plume recirculation is reduced with an increase in wind speed. The region below the ACSC platform progressively experiences a rise in pressure proportional to the wind speed. As a result hot plume air is driven away from the bottom of the ACSC platform.

Plume recirculation is the dominant contributor to the reduced performance of the ACSC, during negative x-direction winds where performance reductions from ideal performance due to plume recirculation is generally in the order of 7 to 10 %, but could become as high as 17 %. The air is drawn into the ACSC from between and above the boiler houses of the power station.

The air drawn in from above the boiler houses entrains some of the hot plume air on its way to the underside of the ACSC.

7.2.2 Effect of skirts

Improvements are indicated in percentage effectiveness, but refer to the case where no wind mitigation measures are implemented. The effect of skirts on ACSC performance were investigated for the case of positive x-direction winds. It was found that the addition of skirts *sk 1* to *sk 3* improved the volumetric flow through cooling unit 1. However the addition of *sk 1* had an arguably insignificant effect on the flow through cooling unit 2 and reduced the flow through cooling unit 3. Skirts *sk 2* to sk 3 showed a marginal improvement in the effectiveness of the ACSC ranging between a 2 to 9 % performance increase compared to cases where no skirts were implemented. The addition of a large elliptical skirt (*sk 4*) did however contribute to a performance increase ranging between 5 to 20 %. This skirt effectively improves the flow through the ACSC by moving the separation region upstream of the fans located near the upstream periphery

7.2.3 Effect of screens and deflection wall

The effects of various screens and a deflection wall on ACSC performance were also investigated for positive x-direction winds. The addition of screens posed a greater contribution to the overall effectiveness of the ACSC compared to skirts. Approaching air is obstructed by the screen beneath the ACSC and is consequently forced upwards into the ACSC. The implementation of screens significantly reduce separation at the upstream periphery, as well as plume recirculation. Performance enhancement due to screens is in the order of 8 % for wind speeds as low as 3 m/s, but increases to approximately 30 % for wind speeds of 9 m/s compared to cases where no screens are implemented.

The deflection wall (*sk 6*) contributed to the improvement of the flow through the Large ACSC in the same manner that a screen of the same height (*sk 1*) did. Further investigation should be done into different deflection wall heights.

7.2.4 Effect of skirt-screen combinations

The effect of two skirt-screen combinations was also investigated for various wind speeds leading to the following conclusions:

For a positive x-direction wind, combination 1 rendered a similar overall effectiveness compared to the results obtained when screen *sc 4* was implemented alone. The implementation of combination 2 rendered an improvement

between 0 and 2 % compared to the implementation of screen *sc 4* alone.

For a negative y-direction wind, combination 1 and 2 improved the volumetric flow through cooling unit 1, but reduced the flow through unit 2. Regardless of this a nett increase in effectiveness, ranging between 1 and 6 %, is seen between these two units. Arguably the implemented skirt-screen combinations had a negligible effect on the effectiveness of units 3 to 6.

The effect of a positive x-direction wind on the performance of the Large ACSC, taking the placement of the power station buildings into account and implementing combinations 1 and 2 showed that a slight reduction in performance occur, compared to the results of the same simulation, excluding the effect of the building. The reduction in performance is between 2 and 3 %. The screen effectively obstructs the approaching flow beneath the ACSC and consequently air also needs to be drawn into the ACSC from the downwind side, where the power station building is located. The building obstructs some of this flow and consequently a marginal reduction in ACSC performance is seen.

Finally the effect of a negative x-direction wind on the performance of the ACSC due to the implementation of combinations 1 and 2 as well as the power station buildings was determined. Generally combination 2 showed a superior increase in performance compared to combination 1 as well as the case of no skirts and screens. The performance is however still lower than the results obtained for the same skirt-screen combinations, excluding the effect of the building.

The previous two paragraphs indicate that a better ACSC performance might be possible if the proximity between the ACSC and the power station building was increased. The implementation of skirt-screen combinations does however always render an effectiveness higher than 90 % for all the cooling units in the ACSC, regardless of the wind direction.

7.3 Further research

Among the answers obtained in the research many questions also arose regarding certain aspects of the ACSC performance. Further research possibilities are as follow:

Modelling of diagonal (xy-direction) winds: Due to the limited amount of computational power available the Large ACSC could only be modeled using symmetry in the x- and y-directions. However the effect of an xy-direction wind should also be considered in order to observe its influence on the performance of the Large ACSC.

Comparison of a detailed with the simplified ACSC model: The numerical ACSC model in the present study was simplified, consisting of a number of fan-unit models together with velocity boundaries as discussed in chapter 3. A greater amount of computational power would make the detailed modeling of all 384 fan-units possible.

Effect of power station building proximity: An investigation should be done to determine the optimal distance between the Large ACSC and the power station buildings. The closer the ACSC is to the power station buildings, the less traveling distance exists for exhausted steam between the turbine outlet and the condenser inlet. The larger the traveling distance, the more energy losses occur due to friction in the steam duct. However, as this study showed, the condenser requires enough surrounding space in order for a sufficient amount of air to enter the ACSC. This becomes a problem if the wind blows across the power station buildings onto the ACSC. Consequently, an optimum distance between the ACSC and the power station buildings should be investigated numerically by varying the building proximity.

Effect of platform height: An analysis could be done for different platform heights of the Large ACSC in order to obtain an optimal height, essentially minimizing the cost of the ACSC support structure, while a sufficient amount of cooling air is still be provided to the heat-exchanger bundles.

Comprehensive analysis and optimization of screens: This research only investigated the effect of two screen heights with some variations to the porosity of screen level 2. A more detailed analysis of screen heights, porosities and placement beneath the ACSC should be investigated in order to obtain an optimum screen configuration.

Comprehensive analysis of deflection walls: A more comprehensive analysis could be done for deflection walls. The present study investigated the effect of one geometry of the deflection wall. However a higher deflection wall may possibly be able to direct approaching winds upward into the ACSC, exploiting the energy of the wind to provide more effective cooling.

Study into accurate numerical fan model: As discussed previously in the work of (Van der Spuy *et al.*, 2009), the accuracy of the *pressure-jump* fan method, used in the present study, is limited, especially during low flow rates through the fan. Therefore an investigation is required where the flow in the vicinity of the fan is analyzed, both experimentally and numerically. Additionally, a more accurate numerical fan model should be developed.

List of References

Akhtar, S.Z. (2000 October). Parallel condensings systems: Getting a fresh look. Magazine: Cooling Systems. pp 63-68.

Al-Waked, R. and Behnia, M. (2003). The performance of natural draft dry-cooling towers under cross wind: CFD study. In: *Proceedings of the 2nd International Conference on Heat Transfer, Fluid Mechanics and Thermodynamics, Victoria falls, Zambia.*

AMCA (1975). AMCA Standard 210-74, Laboratory methods for testing fans for rating.

Bartz, J.A. and Maulbetsch, J.S. (1981). Are dry-cooled power plants a feasible alternative. *Mechanical Engineering*, pp. 34–41.

Bredell, J.R. (2005). *Numerical investigation of fan performance in a forced draft air-cooled steam condenser.* Master's thesis, Department of Mechanical Engineering, University of Stellenbosch, South Africa.

Bredell, J.R. and Kröger, D.G. (2006). Numerical investigation of fan performance in a forced draft air-cooled steam condenser. *Applied Thermal Engineering*, vol. 26, pp. 846–852.

British Standard 848 (1997). Fans for general purposes: Part1. performance tesing using standardized airways.

Bruneau, P.R.P. (1994). *The design of a single rotor axial flow fan for a cooling tower application.* Master's thesis, Department of Mechanical Engineering, University of Stellenbosch, South Africa.

Cengel, Y. and Boles, M. (2006). *Thermodynamics, An engineering approach.* 5th edn. McGraw-Hill.

Conradie, A.E. (1991 January). *Evaluation of the performance characteristics of forced draft air-cooled heat exchangers and the effect of plume recirculation thereon.* Master's thesis, Department of Mechanical Engineering, University of Stellenbosch, South Africa.

Du Toit, C.G., Thiart, G.D. and Kröger, D.G. (1993 November). Analysis of recirculation in mechanical-draught heat exchangers. In: *Proceedings of the 3rd World conference on experimental heat transfer, fluid mechanics and thermodynamics, Honolulu.*

Duvenhage, K., Vermeulen, J.A., Meyer, C.J. and Kröger, D.G. (1995). Flow distortions at the fan inlet in forced-draft air-cooled heat exchangers. *Applied Thermal Engineering*, vol. 16, pp. 741–752.

EPRI (2005). Air-cooled condenser design, specification and operation guidelines. Tech. Rep., EPRI.

Fluent Inc. (2006 September). *Fluent 6.3.6 - User's guide.* Fluent Inc. Fluent Inc. recently became part of ANSYS software.

Gao, X., Zhang, C., Wei, J. and Yu, B. (2009). Numerical simulation of heat transfer performance of an air-cooled steam condenser in a thermal power plant. *Heat Mass Transfer*, vol. 45, pp. 1423–1433.

Goldschagg, H.B. (1993). Lessons learned from the world's largest forced draft direct air-cooled condenser. EPRI meeting, Washington, USA.

Gu, Z., Chen, X., Lubitz, W., Li, Y. and Luo, W. (2006 June). Wind tunnel simulation of exhaust recirculation in an air-cooled system at a large power plant. *International Journal of Thermal Sciences*, vol. 46, pp. 308–317.

Gu, Z., Li, H., Zhang, W., Li, Y. and Peng, J. (2005 June). Wind tunnel simulation on recirculation of air-cooled condensers of a power plant. *Journal of Wind Engineering and Industrial Aerodynamics*, vol. 93, pp. 509–520.

Hotchkiss, P.J., Meyer, C.J. and von Backström, T.W. (2006). Numerical investigation into the effect of cross-flow on the performance of axial flow fans in forced draught air-cooled heat exchangers. *Applied Thermal Engineering*, vol. 26, pp. 200–208.

Joubert, R. (2010). *Influence of geometric and environmental parameters on air-cooled steam condenser performance.* Master's thesis, Department of Mechanical and Mechatronic Engineering, University of Stellenbosch, South Africa.

Knirsch, H. (July 1991). Dry cooling towers at biggest coal fuel power station. *Modern power systems, Ruislip, England.*

Kröger, D.G. (1989). Reduction in performance due to recirculation in mechanical draft cooling towers. *Heat Transfer Engineering*, vol. 10, pp. 37–43.

Kröger, D.G. (2004). *Air-Cooled Heat Exchangers and Cooling Towers.* PennWell Corporation, Tulsa, USA.

Larinoff, M.W., Moles, W.E. and Reichhelm, R. (1978 22 May). *Design and Specification of Air-Cooled Steam Condensers.* Hudson Products Corporation, Houston, USA.

Liu, P., Huishen, D. and Zhao, W. (2009). Numerical investigation of hot air recirculation of air-cooled condensers at a large power plant. *Applied thermal engineering*, vol. 29, pp. 1927–1934.

Meyer, C.J. (2005 January). Numerical investigation of the effect of inlet flow distortions on forced draught air-cooled heat exchanger performance. *Applied Thermal Engineering*, vol. 25, pp. 1634–1649.

Meyer, C.J. and Kröger, D.G. (2001*a*). Air-cooled heat exchanger inlet flow losses. *Applied Thermal Engineering*, vol. 21, pp. 771–786.

Meyer, C.J. and Kröger, D.G. (2001*b*). Numerical simulation of the flow field in the vicinity of an axial flow fan. *Journal for numerical methods in fluids*, vol. 36, pp. 947–969.

Meyer, C.J. and Kröger, D.G. (2003). Numerical investigation of the effect of fan performance on forced draught air-cooled heat exchanger plenum chamber aerodynamic behaviour. *Applied thermal engineering*, vol. 24, pp. 359–371.

Monroe, R.C. (1979 May). Improving cooling tower fan system efficiencies. *Combustion*, vol. 50, no. 11, pp. 20–26.

Owen, M.T.F. (2010 March). *A numerical investigation of air-cooled steam condenser performance under windy conditions*. Master's thesis, Department of Mechanical and Mechatronic Engineering, University of Stellenbosch, South Africa.

Pretorius, J. and Du Preez, A. (2009). Eskom cooling technologies. In: *Proceedings of the 14th IAHR cooling tower conference, Stellenbosch, South Africa*.

Salta, C.A. and Kröger, D.G. (1995). Effect on inlet flow distortions on fan performance in forced draft air-cooled heat exchangers. *Heat recovery systems and CHP*, vol. 15, pp. 555–561.

Stinnes, W.H. and Von Backström, T.W. (2002 April). Effect of cross-flow on the performance of air-cooled heat exchanger fans. *Applied thermal engineering*, vol. 22, pp. 1403–1415.

Swanekamp, R. (2002 September). Cooling options change for a hot thirsty industry. *Power*, vol. 146, pp. 55–60.

Tawney, R., Khan, Z. and Zachary, J. (2005). Economic and Performance Evaluation of Heat Sink Options in Combined Cycle Applications. *Journal of Engineering for Gas Turbines and Power*, vol. 127, pp. 397–403.

Thiart, G.D. and Von Backström, T.W. (1993). Numerical simulation of the flow field near an axial flow fan operating under distorted inflow conditions. *Journal of wind engineering and industrial aerodynamics*, vol. 45, pp. 189–214.

Van Aarde, D.J. (1990 April). *Vloeiverliese deur 'n A-raam vinbuisbundel in 'n lugverkoelde kondensator*. Master's thesis, Department of Mechanical Engineering, University of Stellenbosch, South Africa.

Van der Spuy, S.J., Von Backström, T.W. and Kröger, D.G. (2009 July-August). Performance of low noise fans in power plant air-cooled steam condensers. *Noise control engineering*, vol. 57, pp. 1–7.

Van Rooyen, J.A. (2007). *Performance trends of an air-cooled steam condenser under windy conditions*. Master's thesis, Department of Mechanical Engineering, University of Stellenbosch, South Africa.

Van Rooyen, J.A. and Kröger, D.G. (2008). Performance trends of an air-cooled steam condenser under windy conditions. *Journal of engineering for gas turbines and power*, vol. 130, pp. 023006–1 – 023006–7.

VDI (1978). VDI Guidelines, VDI 2049, Thermal acceptance and performance tests on dry-cooling towers.

Versteeg, H.K. and Malalasekera, W. (2007). *An introduction to computational fluid dynamics - The finite volume method*. 2nd edn. Pearson Education Limited, England.

Appendices

Appendix A

Specifications

A.1 Specifications for the *Van Rooyen (2007)* ACSC

A.1.1 Atmospheric and steam design conditions

Air temperature (dry-bulb):	$T_a = 15.6$ °C (288.75 K)
Barometric pressure:	$p_a = 90000$ N/m^2
Steam temperature:	$T_v = 60$ °C (333.15 K)

A.1.2 Properties of air at the design condition

The thermo-physical properties of air, evaluated at the the design conditions as stated above using the property correlations given by Kröger (2004):

Density:	$\rho_a = 1.0857$ kg/m^3
Thermal conductivity:	$k_a = 0.02535$ W/m.K
Specific heat:	$c_{pa} = 1006.609$ J/kg.K
Molecular viscosity:	$\mu_a = 1.7948(10)^{-5}$ kg/m.s
Prandtl:	$Pr_a = 0.713$

A.1.3 ACSC platform and A-frame specifications

The dimension labels and layout of a general ACSC is depicted in figure A.1 as a reference for the *Van Rooyen* ACSC dimensions given below.

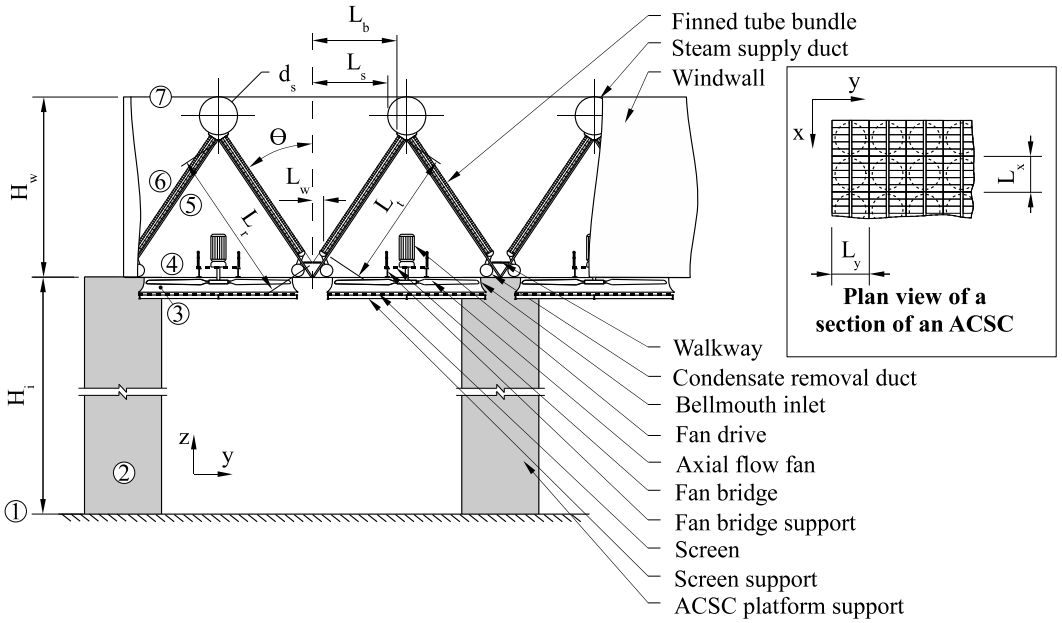

Figure A.1: Platform and A-frame dimensions of an ACSC

Average steam supply duct diameter:	$d_s = 2.34$ m
Half width of the walkway between A-frames:	$L_w = 0.397$ m
Windwall height:	$H_w = 10$ m
Fan platform height above ground level:	$H_i = 20$ m
Apex angle of an A-frame:	$2\theta = 56°$
Dimension r (figure A.1):	$L_r = 10.6$ m
Dimension b (figure A.1):	$L_b = 4.924$ m
Dimension s (figure A.1):	$L_s = 4.102$ m
Dimension x (figure A.1):	$L_x = 10.56$ m
Dimension y (figure A.1):	$L_y = 11.8$ m

A.1.4 Finned tube bundle specifications

Number of finned tube bundles serviced by one fan:	$n_b = 8$
Number of tube rows per bundle:	$n_r = 2$
Number of tubes in upstream row (row 1):	$n_{tb(1)} = 57$
Number of tubes in downstream row (row 2):	$n_{tb(2)} = 58$
Effective finned tube length:	$L_t = 9.55$ m
Frontal area of a single bundle:	$A_{fr} = 27.434$ m^2
Ratio of minimum to free stream flow area through finned tube bundle:	$\sigma = 0.41$
Ratio of minimum to free stream flow area at inlet of finned tube bundle:	$\sigma_{21} = 0.86$

The individual characteristic *heat transfer parameter*, Ny, for row 1 and 2 of the finned tube bundle was determined through experimental analysis and is respectively given below as a function of *flow parameter*, Ry.

$$Ny_{(1)} = 583.8307 Ry^{0.4031}, \quad 1/m \tag{A.1.1}$$

and

$$Ny_{(2)} = 1277.72 Ry^{0.3806}, \quad 1/m \tag{A.1.2}$$

The finned tube bundle loss coefficient for normal flow under isothermal conditions is given as

$$K_{he} = 4464.831 Ry^{-0.439275} \tag{A.1.3}$$

The *heat transfer parameter*, Ny, and *flow paramater*, Ry, are defined by Kröger (2004) as

$$Ny = \frac{hA}{k_a A_{fr} Pr^{0.333}}, \quad 1/m \tag{A.1.4}$$

and

$$Ry = \frac{m_a}{\mu_a A_{fr}}, \quad 1/m \tag{A.1.5}$$

respectively.

A.1.5 Fan specifications

The B-Fan (Bredell, 2005) was used in the investigation of the *Van Rooyen* ACSC. Fan specifications as well as the proximity of various obstructions, found in Joubert (2010), are given below.

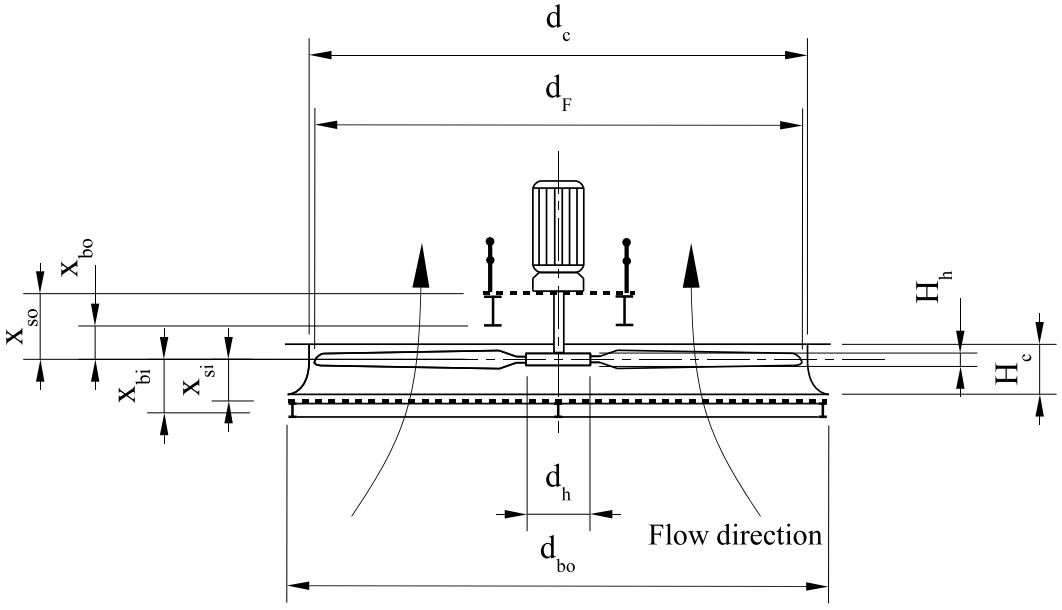

Figure A.2: Fan dimensions and obstruction distances

Fan diameter:	$d_F = 9.145$ m
Casing diameter:	$d_c = 9.216$ m
Casing height:	$H_c = 1.92$ m
Bellmouth outer diameter:	$d_{bo} = 10.134$ m
Hub diameter:	$d_h = 3.658$ m
Hub height:	$H_h = 0.9145$ m
Fan rotational speed:	$N = 125$ rpm
Blade angle (based on chord line, measured at hub):	$\zeta_{cr} = 34.5°$

Inlet screen distance from fan blade (upstream):	$x_{si} = 1.29$ m
Support beam distance from fan blade (upstream):	$x_{bi} = 1.34$ m
Support beam distance from fan blade (downstream):	$x_{bo} = 0.53$ m
Fanbridge distance from fan blade (downstream):	$x_{wo} = 1$ m
Ratio of inlet screen area to fan casing area:	$\sigma_{si} = 0.109$
Ratio of upstream support beam area to fan casing area:	$\sigma_{bi} = 0.154$
Ratio of downstream support beam area to fan casing area:	$\sigma_{bo} = 0.0523$
Ratio of fanbridge area to fan casing area:	$\sigma_{wo} = 0.0912$

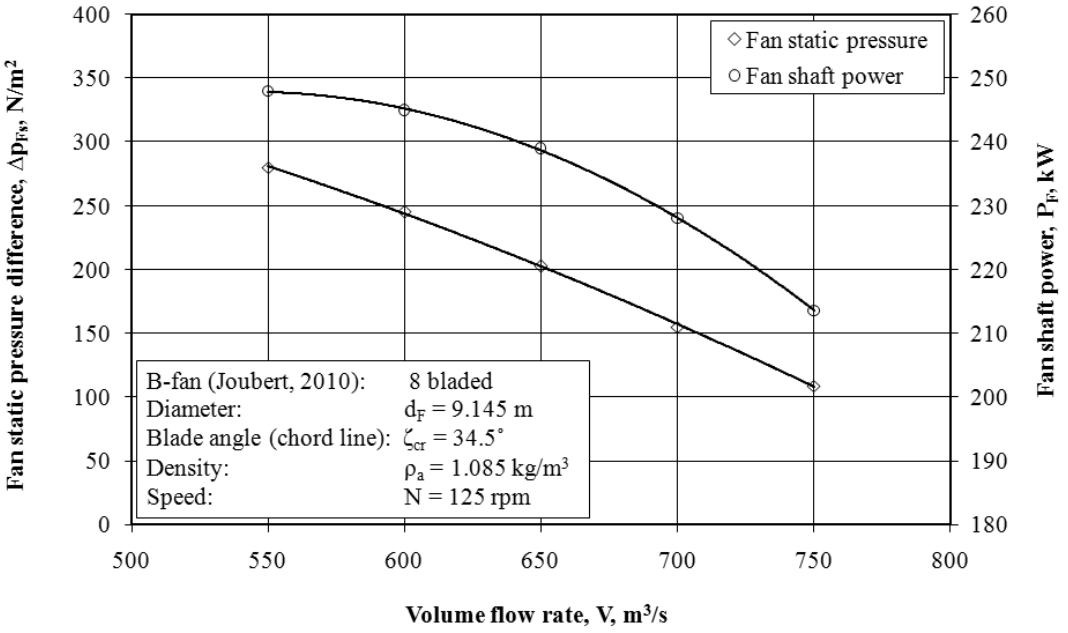

Figure A.3: B-fan characteristic curves (Joubert, 2010)

The fan characteristic curves are given in figure A.3. A second order polynomial fit through the data points in figure A.3 renders the following characteristic equations for the fan static pressure difference, Δp_{Fs}

$$\Delta p_{Fs} = -7.85714(10)^{-4}V^2 + 1.56429(10)^{-1}V + 432.464, \quad N/m^2 \quad \text{(A.1.6)}$$

as well as the fan shaft power, P_F

$$P_F = -8(10)^{-4}V^2 + 8.68(10)^{-1}V + 12.5, \quad kW \quad \text{(A.1.7)}$$

A.1.6 Effective ACSC system losses

A.1.6.1 Description of ACSC system loss coefficients

The effective system flow resistance, Δp_e, through an A-frame heat exchanger between 1 an 7 (figure A.1) is given in section 3.2 and repeated below for convenience:

$$\Delta p_e = -\left(\frac{K_{ts}\left(\frac{m_a}{A_{fr}}\right)^2}{2\rho_{a1}} + \frac{K_{up}\left(\frac{m_a}{A_e}\right)^2}{2\rho_{a3}} + \frac{K_{do}\left(\frac{m_a}{A_e}\right)^2}{2\rho_{a3}} + \frac{K_{\theta t}\left(\frac{m_a}{A_{fr}}\right)^2}{2\rho_{a56}} \right), \quad N/m^2 \tag{A.1.8}$$

In this equation, K_{ts} accounts for the flow loss due to the ACSC platform support structure. K_{up} and K_{do} represents the flow losses due to obstacles in relative close proximity upstream and downstream of the fan. For the fan units considered in the present study the upstream obstacles are the fan inlet screen and the screen support beams. The downstream obstacles are accounted for by the fanbridge as well as the fanbridge support structure. Kröger (2004) presents empirical correlations by which K_{up} and K_{do} can be calculated as a function of the obstacle's projected area and distance from the fan.

Flow losses across the heat exchanger as well as kinetic energy losses at the A-frame heat exchanger outlet (elevation 7, figure A.1) are accounted for by $K_{\theta t}$ and is specified by Kröger (2004) as

$$K_{\theta t} = K_{he} + \left(\frac{1}{\sin\theta_m} - 1\right)\left[\left(\frac{1}{\sin\theta_m} - 1\right) + 2K_{ci}^{0.5}\right] + K_{dj} + K_o \tag{A.1.9}$$

for iso-thermal flow.

K_{he}, the heat exchanger loss coefficient, was previously defined in equation (A.1.3). θ_m is the mean incidence angle of the flow along the face of the heat exchanger and is given by the following emperical relation:

$$\theta_m = 0.0019\theta^2 + 0.9133\theta - 3.1558 \tag{A.1.10}$$

The entrance contraction loss coefficient for turbulent flow between two parallel plates, K_{ci}, based on the upstream velocity is given as

$$K_{ci} = \left(\frac{\left(1 - \frac{1}{\sigma_c}\right)}{\sigma} \right)^2 \tag{A.1.11}$$

where σ is the ratio of flow area between the leading edge of the fins to the equivalent area immediatly upstream of the fins. σ_c is given by another emperical correlation in Kröger (2004) as

$$\begin{aligned}\sigma_c = {} & 0.6144517 + 0.04566493\sigma_{21} - 0.336651\sigma_{21}^2 + 0.4082743\sigma_{21}^3 \\ & + 2.672041\sigma_{21}^4 - 5.963169\sigma_{21}^5 + 3.558944\sigma_{21}^6\end{aligned} \tag{A.1.12}$$

for plate fins.

K_{dj} is the downstream jetting loss coefficient which accounts for some of the mechanical energy loss in the fluid due to a decay in turbulent flow in certain regions downstream of the A-frame heat exchanger bundle. This is given as

$$\begin{aligned}K_{dj} = {} & \left[\left\{ -2.89188 \left(\frac{L_w}{L_t} \right) + 2.93291 \left(\frac{L_w}{L_t} \right)^2 \right\} \left(\frac{L_t}{L_s} \right) \left(\frac{L_b}{L_s} \right) \left(\frac{28}{\theta} \right)^{0.4} \right. \\ & \left\{ exp\left(2.36987 + 5.8601(10)^{-2}\theta - 3.3797(10)^{-3}\theta^2\right) \left(\frac{L_s}{L_b} \right) \right\}^{0.5} \\ & \left. \left(\frac{L_t}{L_r} \right) \right]^2\end{aligned} \tag{A.1.13}$$

Finally, the outlet loss coefficient, K_o, is given as

$$\begin{aligned}K_o = {} & \left[\left\{ -2.89188 \left(\frac{L_w}{L_t} \right) + 2.93291 \left(\frac{L_w}{L_t} \right)^2 \right\} \left(\frac{L_s}{L_b} \right)^3 \right. \\ & \left. + 1.9874 - 3.02783 \left(\frac{d_s}{2L_b} \right) + 2.0187 \left(\frac{d_s}{2L_b} \right)^2 \right] \left(\frac{L_t}{L_s} \right)^2\end{aligned} \tag{A.1.14}$$

A.1.6.2 Evaluation of ACSC system loss coefficients

The various loss coefficients will be evaluated in this section, using the properties given earlier, to obtain the system resistance for the *Van Rooyen* ACSC asuming that the flow remains iso-thermal through the ACSC system. This

is justified since the variation in thermo-physical properties of air is small for the temperature spectrum of $T_{a(inlet)}(15.6\ ^{\circ}C) < T_a < T_v(60\ ^{\circ}C)$.

Through the empirical correlations presented by Kröger (2004), K_{ts}, K_{up} and K_{do} were calculated to be:

$$K_{ts} = 1.60 \quad \text{(based on the heat exchanger frontal area)}$$
$$K_{up} = 0.28$$
$$K_{do} = 0.35$$

The heat exchanger loss coefficient is evaluated according to equations (A.1.3) and (A.1.5) as

$$\begin{aligned} K_{he} &= 4464.831 Ry^{-0.439275} \\ &= 4464.831 \left(\frac{m_a}{(1.7948(10)^{-5})\,(8)(27.434)} \right)^{-0.439275} \\ &= 392.2244 m_a^{-0.43927} \end{aligned}$$

The mean incidence angle and contraction ratio according to equations (A.1.10) and (A.1.12) respectively is

$$\theta_m = 0.0019(28)^2 + 0.9133(28) - 3.1558 = 23.906^{\circ}$$

$$\begin{aligned} \sigma_c &= 0.6144517 + 0.04566493(0.86) - 0.336651(0.86)^2 + 0.4082743(0.86)^3 \\ &\quad + 2.672041(0.86)^4 - 5.963169(0.86)^5 + 3.558944(0.86)^6 \\ &= 0.7617 \end{aligned}$$

The contraction, jetting and outlet loss coefficient can now be calculated using equations (A.1.11), (A.1.13), (A.1.14) respectively as

$$K_{ci} = \left(\frac{\left(1 - \frac{1}{(0.761)}\right)}{(0.41)} \right)^2 = 0.582$$

$$K_{dj} = \left[\left\{ -2.89188 \left(\frac{(0.397)}{(9.55)} \right) + 2.93291 \left(\frac{(0.397)}{(9.55)} \right)^2 \right\} \left(\frac{(9.55)}{(4.102)} \right) \left(\frac{(4.924)}{(4.102)} \right) \left(\frac{28}{(28)} \right)^{0.4} \left\{ exp \left(2.36987 + 5.8601(10)^{-2}(28) \right. \right. \right.$$
$$\left. \left. \left. -3.3797(10)^{-3}(28)^2 \right) \left(\frac{(4.102)}{(4.924)} \right) \right\}^{0.5} \left(\frac{(9.55)}{(10.6)} \right) \right]^2 = 1.664$$

$$K_o = \left[\left\{ -2.89188 \left(\frac{(0.397)}{(9.55)} \right) + 2.93291 \left(\frac{(0.397)}{(9.55)} \right)^2 \right\} \left(\frac{(4.102)}{(4.924)} \right)^3 \right.$$
$$\left. + 1.9874 - 3.02783 \left(\frac{(2.34)}{2(4.924)} \right) + 2.0187 \left(\frac{(2.34)}{2(4.924)} \right)^2 \right] \left(\frac{(9.55)}{(4.102)} \right)^2$$
$$= 7.117$$

Using equation (A.1.9), the kinetic energy loss coefficient can now be calculated in terms of mass flow rate, m_a, as

$$K_{\theta t} = \left(392.2244 m_a^{-0.43927} \right) + \left(\frac{1}{\sin(23.906)} - 1 \right)$$
$$\left[\left(\frac{1}{\sin(23.906)} - 1 \right) + 2(0.582)^{0.5} \right] + (1.664) + (7.117)$$

$$= 392.2244 m_a^{-0.43927} + 13.174$$

Substituting the results obtained for K_{ts}, K_{up}, K_{do} and $K_{\theta t}$ into equation (A.1.8) renders a correlation for the system resistance:

$$\begin{aligned}\Delta p_e = -\Bigg[&\frac{(1.60)\left(\frac{m_a}{(8\cdot 27.434)}\right)^2}{2(1.0857)} + \frac{(0.28)\left(\frac{m_a}{(\frac{\pi}{4}(9.216^2-3.658^2))}\right)^2}{2(1.0857)} \\ &+ \frac{(0.35)\left(\frac{m_a}{(\frac{\pi}{4}(9.216^2-3.658^2))}\right)^2}{2(1.0857)} \\ &+ \frac{(392.2244 m_a^{-0.43927} + 13.174)\left(\frac{m_a}{(8\cdot 27.434)}\right)^2}{2(1.0857)}\Bigg] \\ = -&\left(2.33147(10)^{-4} m_a^2 + 3.74998(10)^{-3} m_a^{1.56073}\right), \quad N/m^2\end{aligned} \tag{A.1.15}$$

The system resistance can be written in terms of volumeflow by substituting equation (A.1.16) into (A.1.15).

$$m_a = V_a \rho_a, \quad kg/s \tag{A.1.16}$$

$$\Delta p_e = -\left(2.7483(10)^{-4} V_a^2 + 4.2636(10)^{-3} V_a^{1.56073}\right), \quad N/m^2 \tag{A.1.17}$$

A.2 Specifications for the Large ACSC

Due to confidentiality the specifications of the Large ACSC are omitted.

Appendix B

Numerical fan model

B.1 Derivation of the *pressure-jump* model

Industrial fans are usually tested in a fan test facility in order to obtain the fan performance characteristics. According to Kröger (2004) various standards exist by which fans should be tested, among which the British standard (British Standard 848, 1997) for fan tesing recognizes four test facility installation types, being type A, B, C and D. A Type A *(free inlet-free outlet)* test facility is commonly used for industrial fan testing. The last section at the end of such a testing facility is depicted in figure B.1.

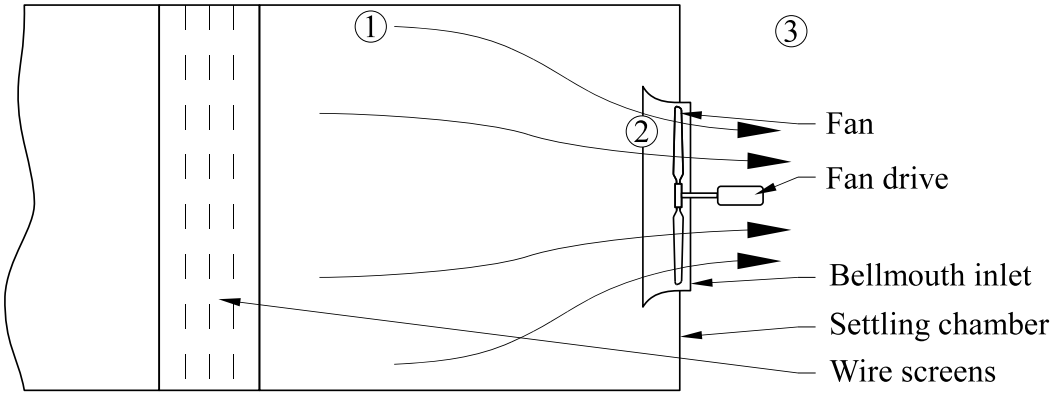

Figure B.1: End section of a BS 848, type A fan test facility

In these test facilities, air is drawn into the settling chamber relatively undistorted, by the fan that is being tested. The wire screens further improve the even flow distribution through the settling chamber. The pressure difference between the settling chamber at 1 and the atmosphere at 3 is then measured for different volume flow rates to give the fan static pressure rise,

Δp_{Fs}, defined by equation (B.1.1).

$$\Delta p_{Fs} = p_{s3} - p_{t1} \tag{B.1.1}$$

where the total pressure, p_t is given in terms of the static and dynamic pressure, p_s and p_d respectively, as

$$\begin{aligned} p_t &= p_s + p_d \\ &= p_s + \frac{\rho v^2}{2} \end{aligned} \tag{B.1.2}$$

For equation (B.1.1), small flow losses due to the settling chamber and bellmouth are neglected.

The *pressure-jump* model in *Fluent* gives a static to static pressure differential, Δp_{Fss}, across a specified plane and therefore requires a static to static pressure characteristic calculated by equation (B.1.3).

$$\Delta p_{Fss} = p_{s3} - p_{s2} \tag{B.1.3}$$

As previously mentioned, minor flow losses due to the settling chamber and bellmouth are neglected and so

$$p_{t2} \approx p_{t1} \tag{B.1.4}$$

Therefore

$$p_{s2} = p_{s1} + \frac{\rho v_1^2}{2} - \frac{\rho v_2^2}{2} \tag{B.1.5}$$

where v_2 is the velocity though the annulus of the fan.

By substituting equation (B.1.5) into (B.1.3), a new expression for the static to static pressure rise between 2 and 3 is obtained:

$$\begin{aligned} \Delta p_{Fss} &= p_{s3} - \left(p_{s1} + \frac{\rho v_1^2}{2} - \frac{\rho v_2^2}{2} \right) \\ &= p_{s3} - p_{t1} + \frac{\rho v_2^2}{2} \\ &= \Delta p_{Fs} + \frac{\rho v_2^2}{2} \end{aligned} \tag{B.1.6}$$

Notably the static to static pressure rise between 2 and 3 is the specified fan static pressure with the added dynamic pressure component of position 2.

B.2 *Pressure-jump* characteristic for the *Van Rooyen* ACSC

Fluent requires a polynomial for the static to static fan pressure difference in terms of the velocity, v, through the annulus of the fan. A second order polynomial was fitted through the data of the *pressure-jump* characteristic of figure B.2. The *pressure-jump* characteristic for the B-fan used in the *Van Rooyen* ACSC is therefore written as

$$\Delta p_{Fss} = -2.63055v^2 + 27.2461v + 323.2303, \quad N/m^2 \tag{B.2.1}$$

valid for

$$5 < v < 15, \quad m/s$$

Fluent allows the user to specify the velocity spectrum in which the *pressure-jump* characteristic is valid. The pressure rise across the specified *pressure-jump* plane is therefore subject to the specified polynomial in this region, but gives a constant pressure rise outside of the specified velocity spectrum, as shown in figure B.2.

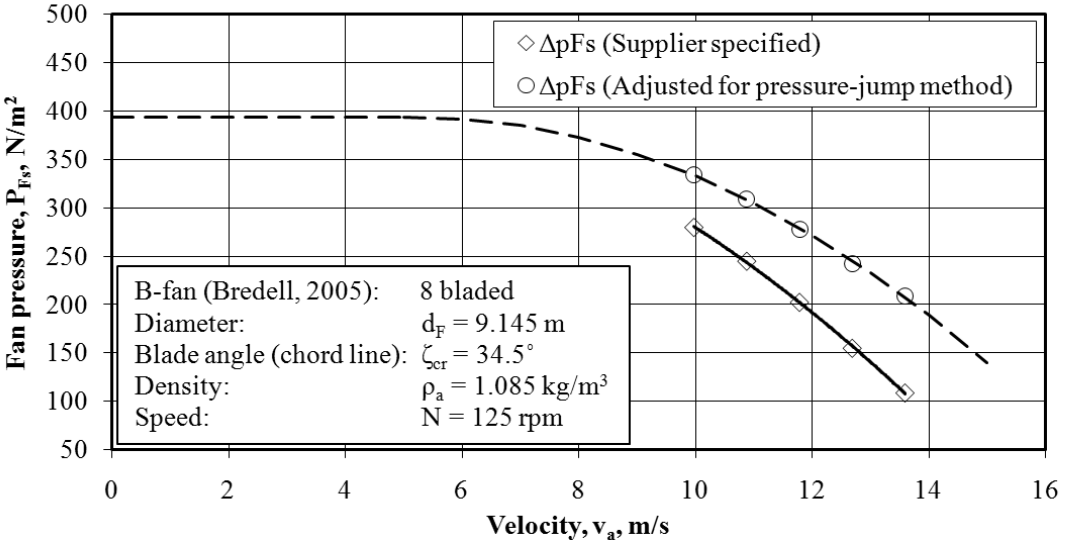

Figure B.2: Fan static and *pressure-jump* characteristic for the B-fan used in the *Van Rooyen* ACSC

B.3 *Pressure-jump* characteristic for the Large ACSC

The *pressure-jump* characteristic for the fan used in the Large ACSC was determined in a similar manner to the fan characteristic of the *Van Rooyen* ACSC, but omitted due to confidentiality.

Appendix C

Numerical heat exchanger model

The numerical model for a single fan unit is depicted in figure C.1 (The dimensions, excluding L_z, are given in appendix A). This model, initially proposed by Bredell (2005), models the heat transfer and pressure loss through a single A-frame fan unit by means of a rectangular plenum chamber with a horizontal (xy-plane) downstream heat exchanger at the end of the plenum. The heat exchanger is modeled by means of a porous media in *Fluent*. This requires the calculation of two attributes i.e. the numerical momentum sink terms and the heat source terms, which serve as input values to the *Fluent* porous model for the numerical calculaton of the pressure difference across the heat exchanger as well as the heat transfer to the fluid. Hence, the analysis of the mentioned attributes is detailed below.

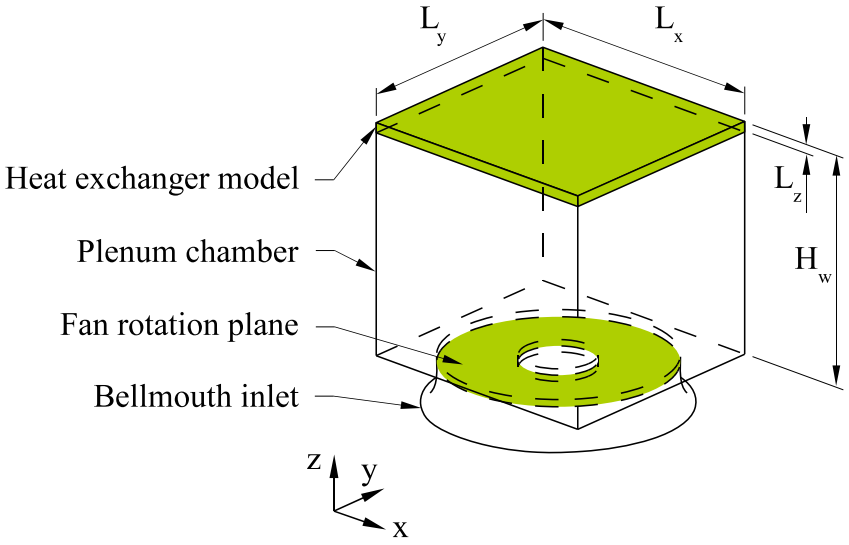

Figure C.1: Numerical fan unit model

C.1 Numerical pressure loss model

In the numerical fan unit model shown in figure C.1, subsystems of the A-frame heat exchanger such as fan drives, walkways, screens and support beams are not modeled explicitly, since the effect of plenum flow characteristics are not in the scope of this study. This detail could lead to unnecessary large and complex computational mesh sizes, being computationally expensive. Instead, the pressure difference occuring in the flow due to these subsystems are captured in the draft equation (A.1.8), which represents the effective system resistance.

The numerical fan unit model incorporates the effective system resistance through momentum sink terms in the heat exchanger model (*Fluent* porous media). This requires the calculation of the inertial and viscous loss coefficients, which serves as input values for the *Fluent* porous media. The walls of the fan unit plenum are modeled as slip walls, allowing no pressure difference to occur due to surface roughness. The evaluation of the numerical loss coefficients for the *Van Rooyen (2007)* fan-unit follows below, but are omitted for the Large fan-unit due to confidentiality.

C.1.1 Evaluation of numerical loss coefficients for the *Van Rooyen (2007)* ACSC

The effective system resistance given by equation (A.1.17) can be approximated by a second order polynomial as

$$\Delta p_e \approx -\left(4.1636(10)^{-4}V_a^2 + 7.4120(10)^{-2}V_a\right) \quad , N/m^2 \tag{C.1.1}$$

The volume flow through the heat exchanger can also be given as a function of the z-direction velocity, w, as

$$V_a = |w|\,(L_x \cdot L_y) \quad , m^3/s \tag{C.1.2}$$

A relation for Δp_e in terms of, w, is obtained by substituting equation (C.1.2) into (C.1.1).

$$\begin{aligned}\Delta p_e &= -\left(4.1636(10)^{-4}|w|w\,(L_x \cdot L_y)^2 + 7.4120(10)^{-2}w\,(L_x \cdot L_y)\right)\\ &= 4.1636(10)^{-4}|w|w\,((11.8)(10.56))^2\\ &\quad + 7.4120(10)^{-2}w\,((11.8)(10.56))\\ &= 6.4649|w|w + 9.2360w \quad , N/m^2\end{aligned} \tag{C.1.3}$$

For a heat exchanger porous model thickness of $L_z = 0.2\ m$, the z-direction body force, F_z, acting on the fluid passing through the model can be calculated by

$$F_z = \frac{\Delta p_e}{L_z} = \frac{(6.4649|w|w + 9.2360w)}{(0.2)} = 32.3244|w|w + 46.1799w \quad , N/m^3 \tag{C.1.4}$$

According to Bredell (2005) the body force acting in the z-direction can be defined as

$$F_z = \left(C_z \frac{1}{2} \rho |\mathbf{v}| w + \frac{\mu}{\alpha_z} w \right) \quad , N/m^3 \tag{C.1.5}$$

However, since the flow in the x- and y-direction is restricted through the heat exchanger, $|\mathbf{v}| \approx |w|$, and therefore the inertial and viscous loss coefficients, C_z and $1/\alpha_z$ respectively, can be calculated as follow:

$$\begin{aligned} C_z \rho / 2 &= 30.1693 \\ C_z &= 59.5447 \quad , 1/m \end{aligned} \tag{C.1.6}$$

and

$$\begin{aligned} \mu / \alpha_z &= 46.1799 \\ 1/\alpha_z &= 2.440231(10)^6 \quad , 1/m^2 \end{aligned} \tag{C.1.7}$$

To constrict the flow through the heat exchanger porous model in the z-direction (vertical), the inertial loss coefficients, C_y and C_x are chosen to be $C_z \cdot (10)^3$.

C.1.2 Evaluation of numerical loss coefficients for the Large ACSC

The viscous and inertial loss coefficients for the Large ACSC are calculated similarly to the coefficients of the *Van Rooyen (2007)* ACSC, but omitted due to confidentiality.

C.2 Numerical heat transfer model

The heat transfer model, simulates the heat transfered by the ACSC heat exchanger bundles to the cross-flowing air. This heat transfer was modeled by

implementation of a *user defined function (UDF)* in *Fluent*.

A *UDF* allows the user to program a seperate set of calculations in programming language *C*, that will be used to calculate certain values for implimentation in *Fluent*. This *UDF* can then be read into *Fluent* during the original configuration of the numerical model, whereafter it will be executed during each iteration.

The *UDF* computing the heat source terms through the heat exchanger porous model (shown in figure C.1), extracts the temperature and massflow through each cell immediately downstream of the model. These values are then used to calculate the heat source terms to be added to the air that flows through the porous model during each iteration. These heat source terms are calculated as shown below.

The heat transfer rate, $Q_{(1)}$, is calculated by means of the $e-NTU$ method and is given as

$$Q_{(1)} = m_a c_{pa} \left(T_{ao(1)} - T_{ai(1)}\right) = e_{(1)} m_a c_{pa} \left(T_s - T_{ai(1)}\right) \quad ,W \tag{C.2.1}$$

for the first tube row.

Distortion of air flow in the plenum chamber of the numerical fan-unit, causes numerical diffusion between the cells in and immediately upstream of the heat-exchanger model that would return a faulty air inlet temperature to the *UDF*. This significantly decreases the heat transfer rate to the air and subsequently the air outlet temperature. To mitigate this error, $T_{ai(1)}$ was taken as the average air temperature at the fan rotation plane.

Rearranging equation (C.2.1) in terms of the outlet temperature, $T_{ao(1)}$, gives

$$T_{ao(1)} = e_{(1)} \left(T_s - T_{ai(1)}\right) + T_{ai(1)} = e_{(1)} T_s + \left(1 - e_{(1)}\right) T_{ai(1)} \quad ,K \tag{C.2.2}$$

where $e_{(1)}$ is the effectiveness of the first tube row and can be calculated according to

$$e_{(1)} = 1 - e^{\left(\frac{-UA_{(1)}}{m_a c_{pa}}\right)} \tag{C.2.3}$$

The overall heat transfer coefficient for the first tube row, $UA_{(1)}$, can be approximated by the air-side convection heat transfer cofficient, $h_a A_{(1)}$, since the thermal resistance of the condensate film on the inside of the tube is very small

in comparison to the overall resistance (in the order of 2 %, (Kröger, 2004)). Therefore

$$UA_{(1)} \approx h_a A_{(1)} \quad , J/K \tag{C.2.4}$$

where $h_a A_{(1)}$ is adapted from equation (A.1.4) and given as

$$h_a A_{(1)} = k_a A_{(1)} N y_{(1)} P_r^{0.333} \quad , J/K \tag{C.2.5}$$

and

$$A_{(1)} = \frac{n_{tb(1)}}{n_{tb(2)}} n_b A_{fr} \quad , m^2 \tag{C.2.6}$$

The characteristic heat transfer parameter, $Ny_{(1)}$, requires the calculation of the characteristic flow parameter, $Ry_{(1)}$, which is taken from equation (A.1.5) as

$$Ry = \frac{m_a}{\mu_a A_{(1)}} \quad , 1/m \tag{C.2.7}$$

The heat transfer rate of the second tube row, $Q_{(2)}$, can be calculated in a similar manner to the first bearing in mind that the air temperature leaving the first tube row is equal to the air temperature entering the second tube row ($T_{ao(1)} = T_{ai(2)}$). Similarly the frontal area of the second tube row is the same as the heat exchanger frontal area as given in appendix A ($A_{(2)} = A_{fr}$). The temperature of air leaving the second tube row can now be calculated from

$$\begin{aligned} T_{ao(2)} &= e_{(2)} T_s + \left(1 - e_{(2)}\right) T_{ai(2)} \\ &= e_{(2)} T_s + \left(1 - e_{(2)}\right) \left[e_{(1)} T_s + \left(1 - e_{(1)}\right) T_{ai(1)}\right] \quad , K \end{aligned} \tag{C.2.8}$$

The total heat transfer rate per fan unit can subsequently be given as

$$Q_{tot} = Q_{(1)} + Q_{(2)} = m_a c_{pa} \left(T_{ao(2)} - T_{ai(1)}\right) \quad , W \tag{C.2.9}$$

The heat source terms, S_e, added to the flow through the heat exchanger can now be calculated and is defined as

$$S_e = \frac{\delta Q}{\delta V} \quad , W/m^3 \tag{C.2.10}$$

By substitution of equation (C.2.9) into (C.2.10), the following relation for the

numerical heat exchanger source terms is produced

$$S_e = \frac{\delta m_a}{\delta V} c_{pa} \left(T_{ao(2)} - T_{ai(1)} \right) = \frac{\rho_a |w|}{L_z} c_{pa} \left(T_{ao(2)} - T_{ai(1)} \right) \quad , W/m^3 \quad \text{(C.2.11)}$$

Appendix D

Large ACSC numerical model details

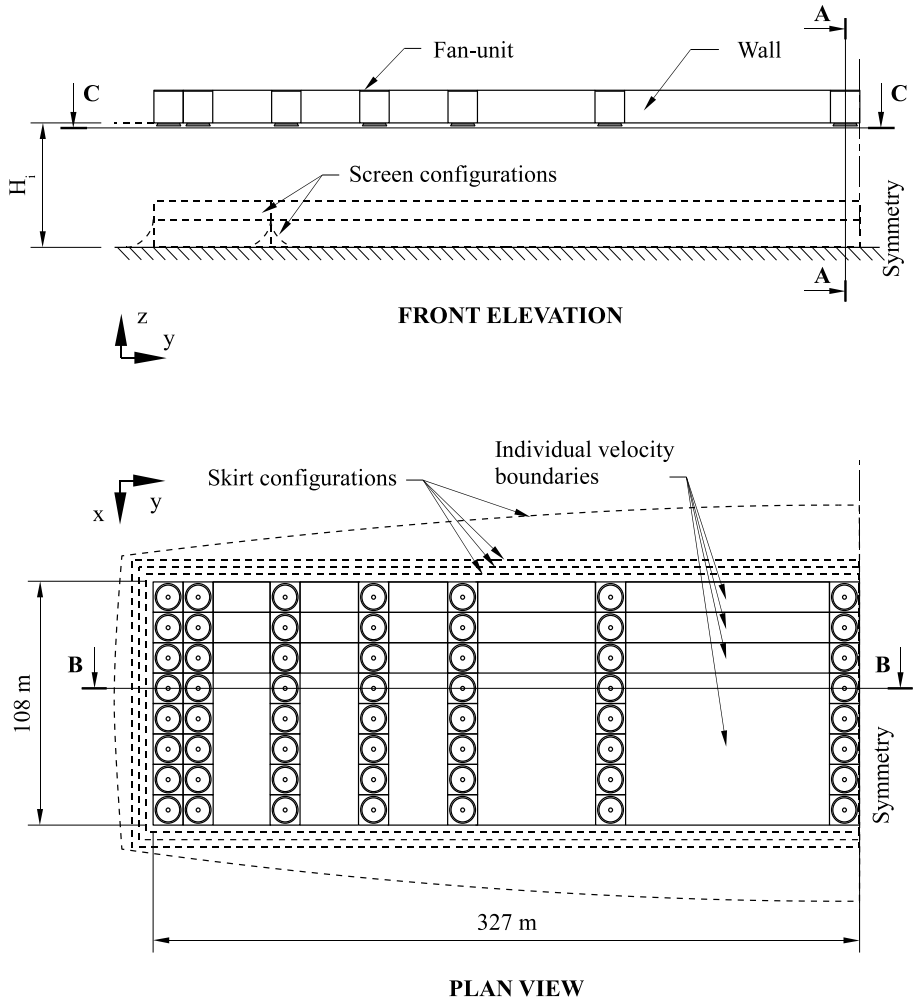

Figure D.1: Details regarding the ACSC model in the x-direction wind domain

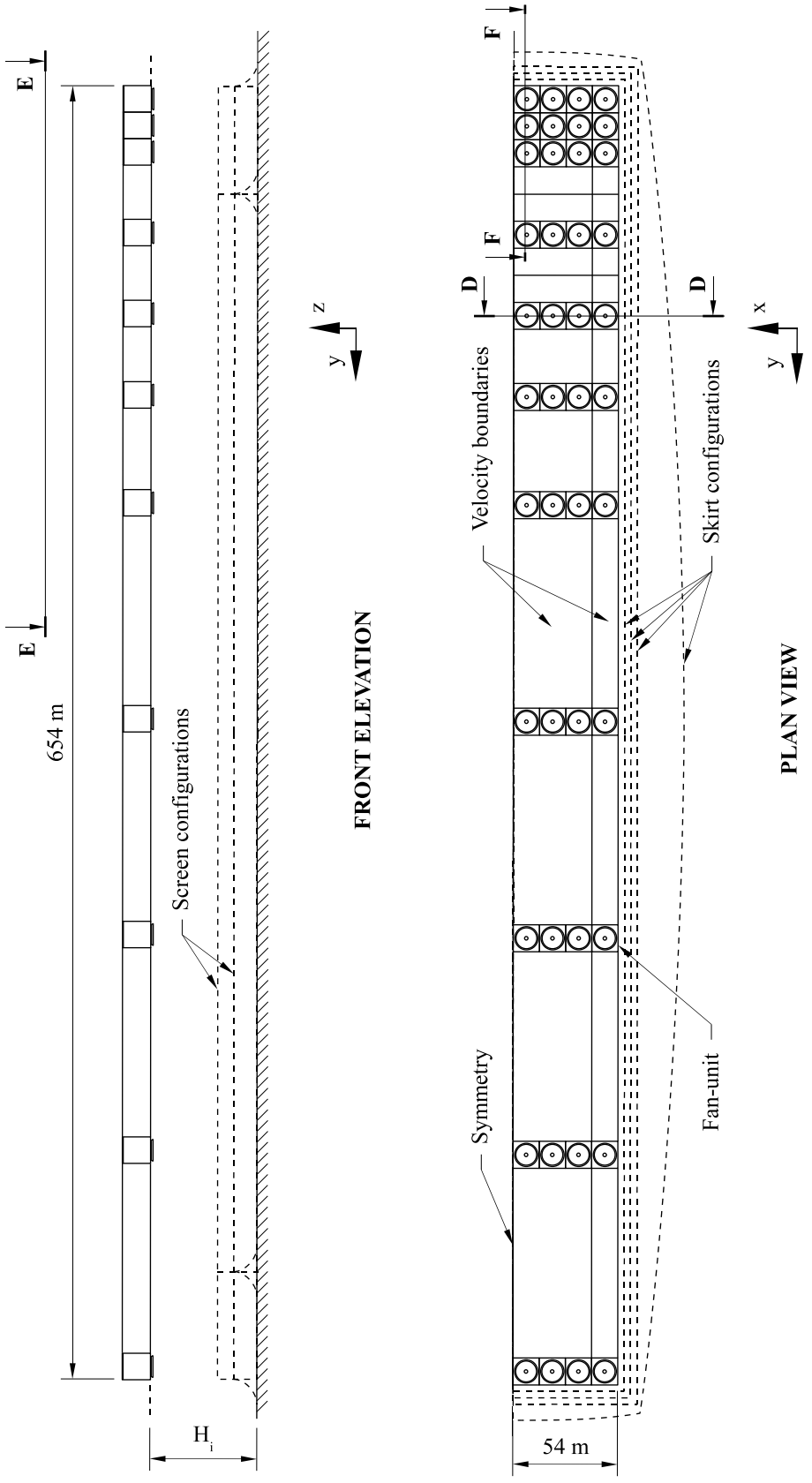

Figure D.2: Details regarding the ACSC model in the y-direction wind domain

Appendix E

Interpolation scheme

Due to the computational limitation of the present study, only some fan-units were physically modeled. The flow and inlet air temperatures for fan-units not modeled were interpolated between adjacent fan-units by means of a linear interpolation scheme explained together with figure E.1. The simulated results obtained for the volumetric flow rates through all the modeled fan-units in the ACSC, were used as end point values for a line. The volumetric flow rate for the number of fan-units in between two consecutive fan-units, were obtained by linearly interpolating between the end point values. Interpolation was only done in the y-direction.

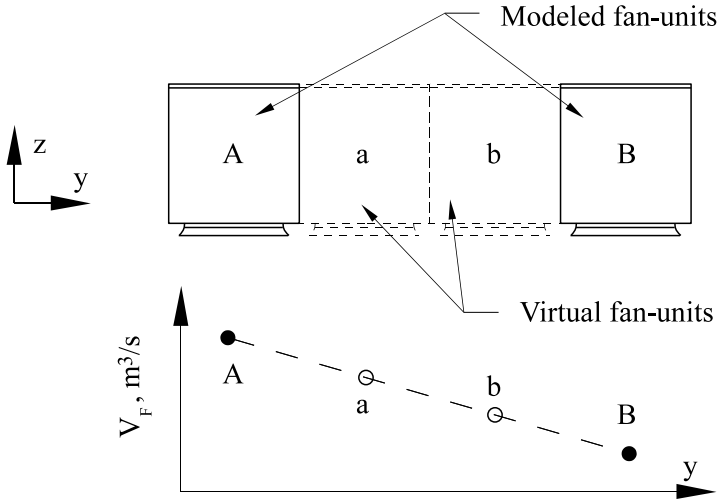

Figure E.1: Illustration of the linear interpolation scheme used in the present study

Figure E.2 presents an example where a curve fit was done through the numerically obtained flow rates (labeled as original) of the fans in row 1, where the free standing ACSC was subject to a 3, 6 and 9 m/s positive x-direction wind. The linearly interpolated values (labeled as interpolated) are also added

to the figure, showing good correlation with the fitted curve.

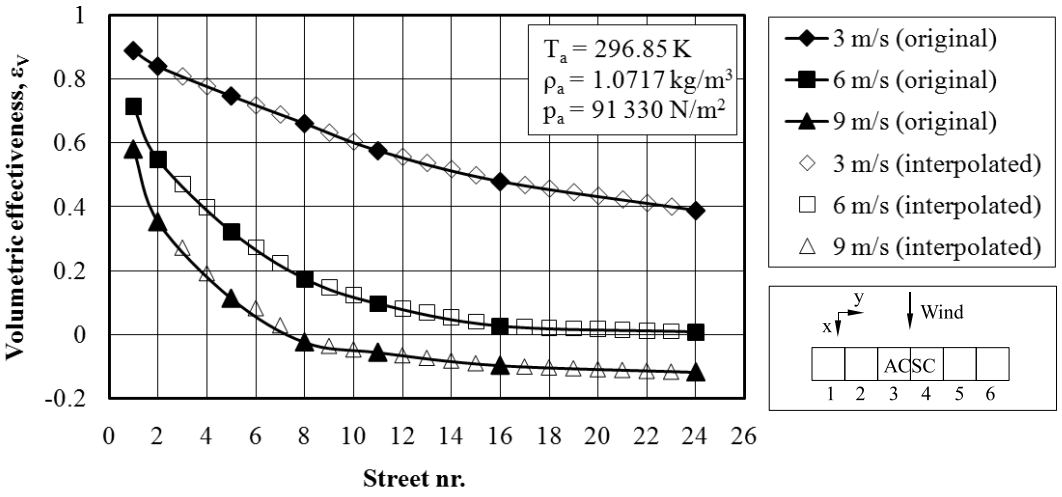

Figure E.2: Numerical and interpolated values for the volumetric flow rates through individual fan units in row 1 compared to a curve fit through numerically obtained values for a 3, 6 and 9 m/s x-direction wind

Appendix F

Overall effectiveness results for skirts and screens

The effect of various skirts, screens and combinations of these on the overall perfromance of the Large ACSC under wind is shown in this appendix with reference to the discussion in chapter 6.

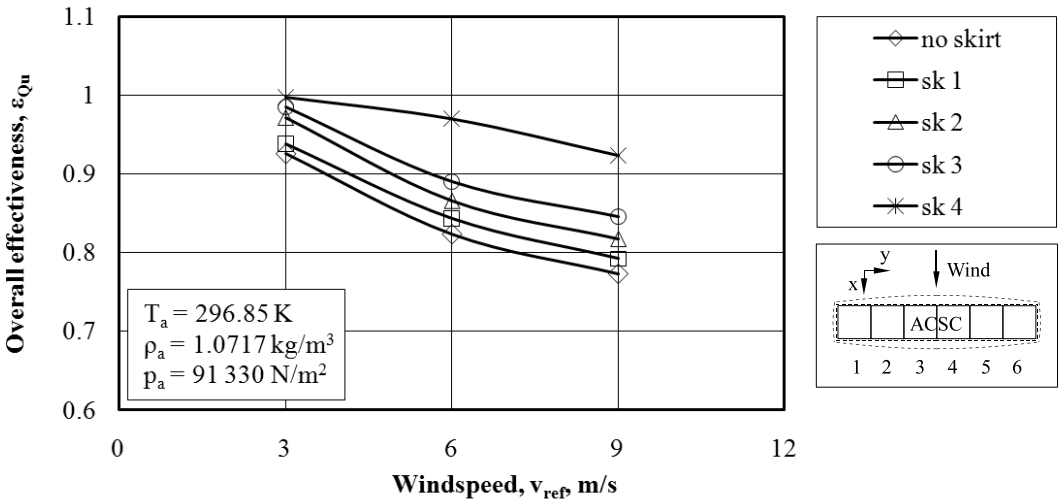

(a)

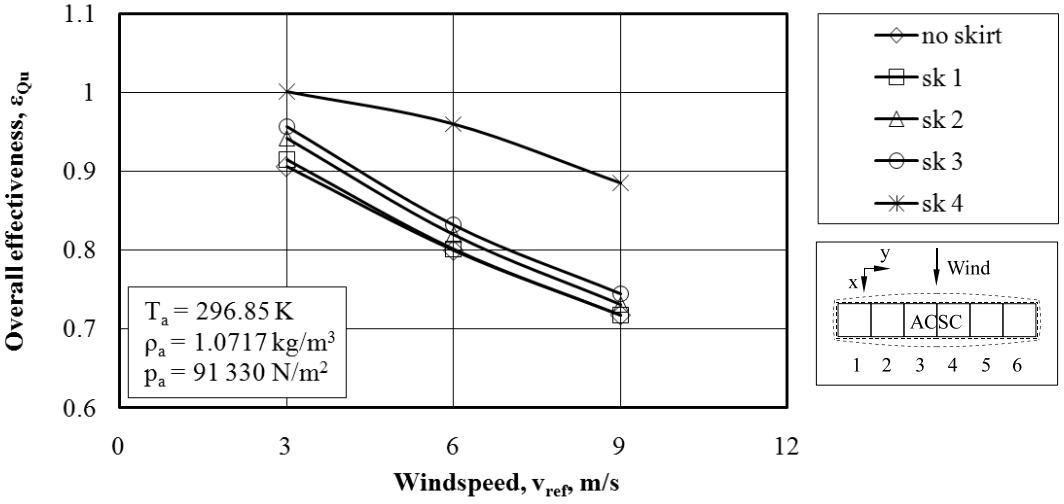

(b)

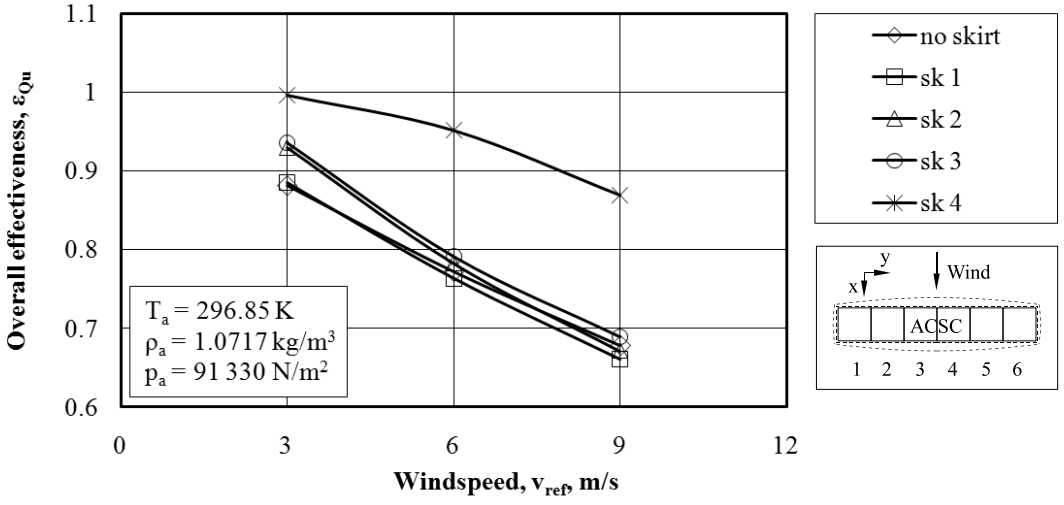

(c)

Figure F.1: The effect of various skirts on the overall effectiveness of (a) unit 1, (b) unit 2 and (c) unit 3 for positive x-direction winds

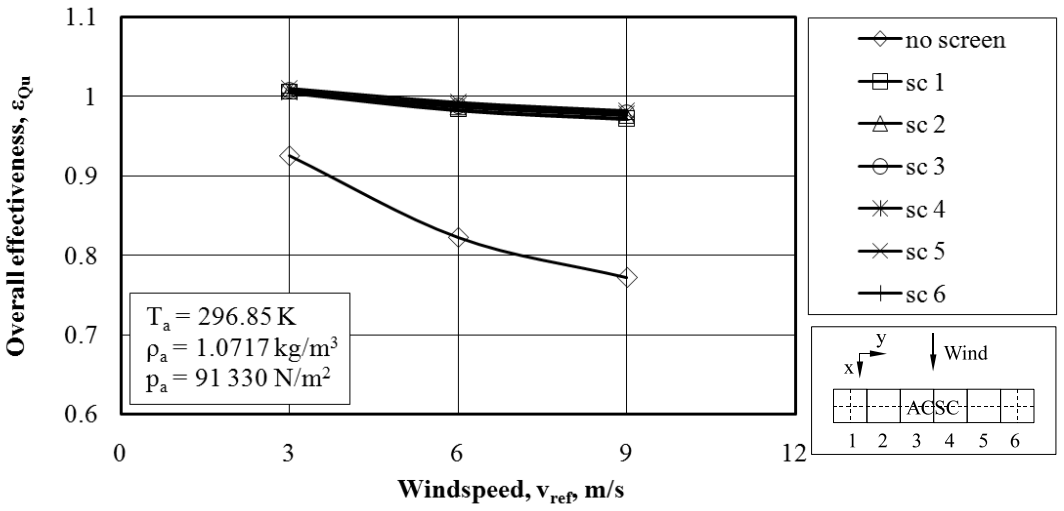

(a)

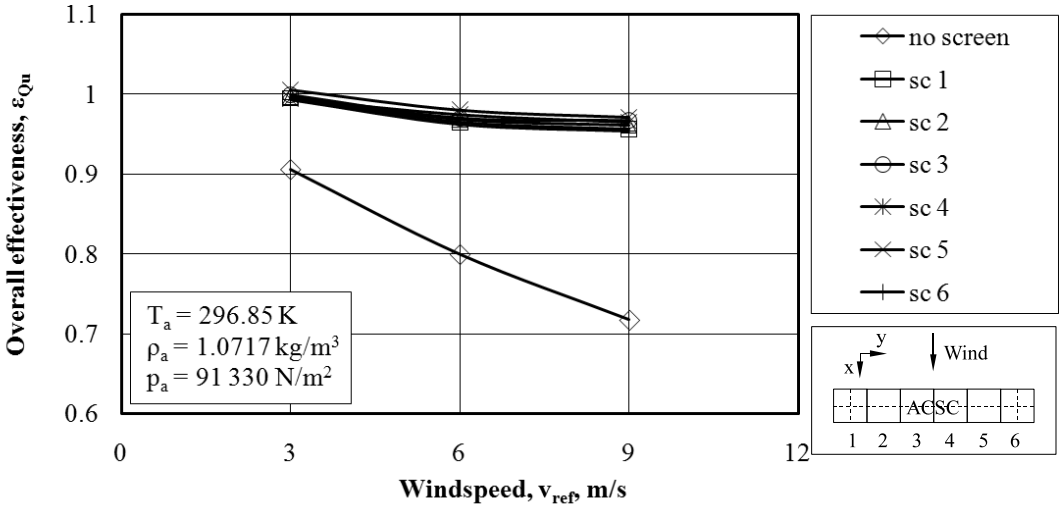

(b)

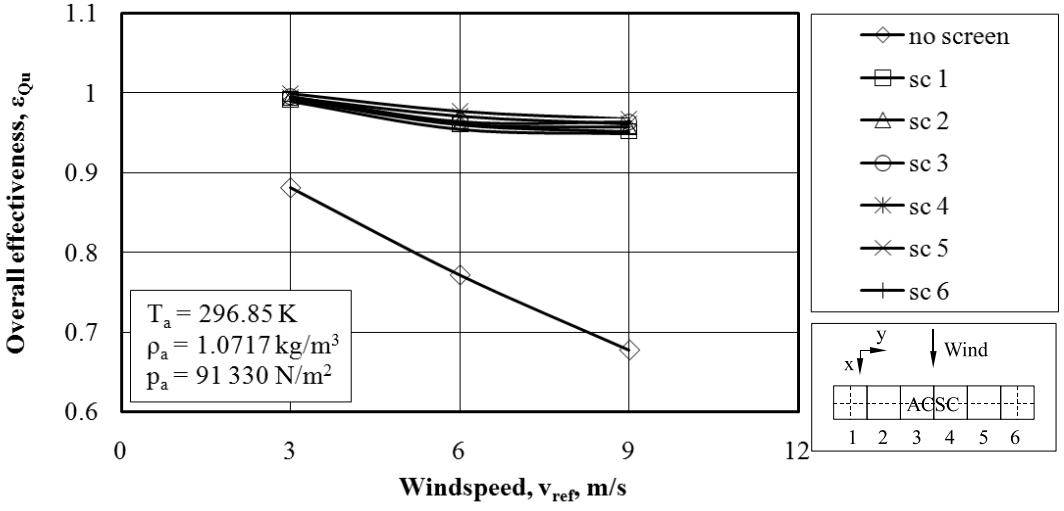

(c)

Figure F.2: The effect of various screens on the overall effectiveness of (a) unit 1, (b) unit 2 and (c) unit 3 for positive x-direction winds

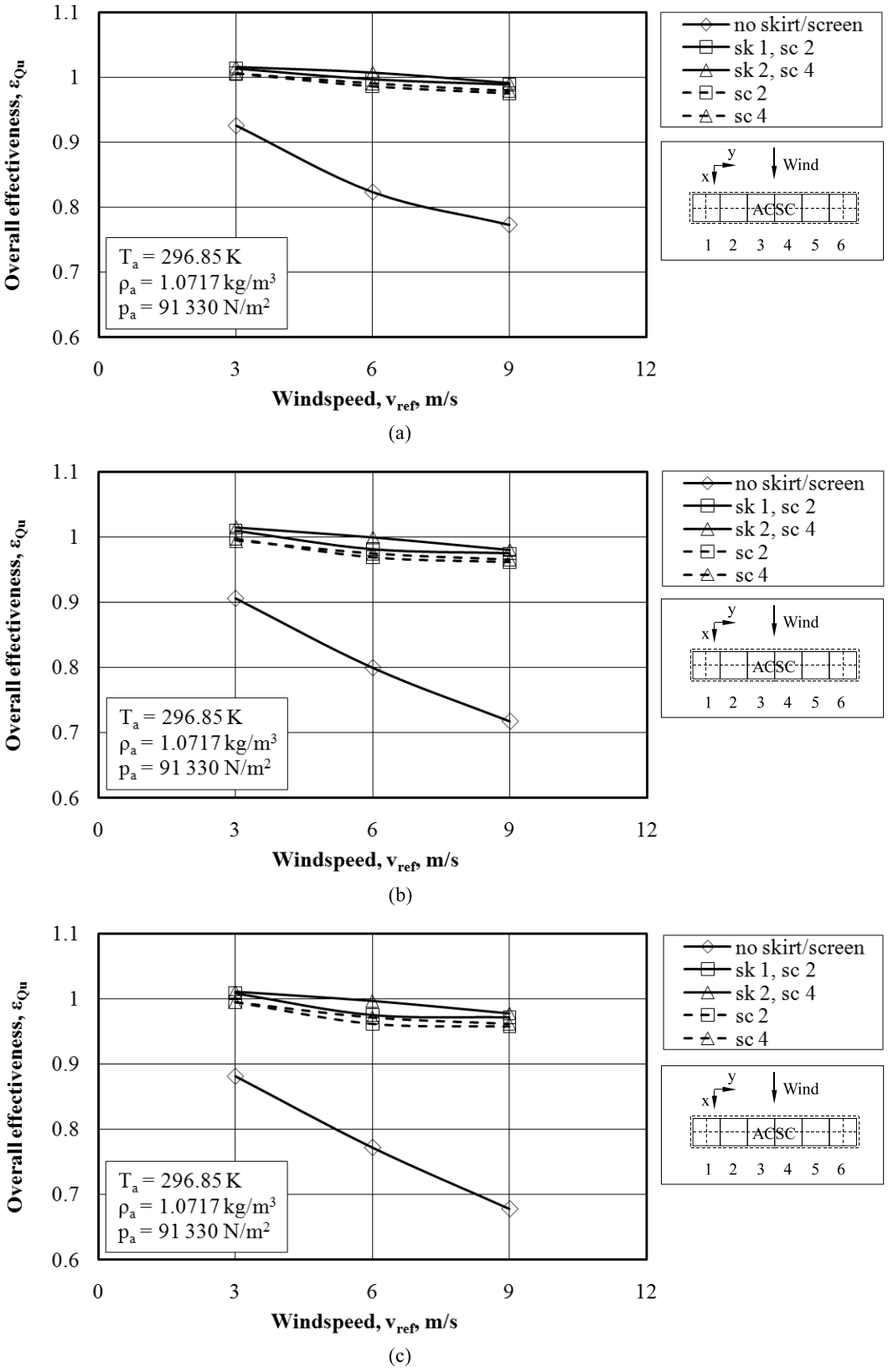

Figure F.3: The combined effect of various skirt-screen configurations on the overall effectiveness of (a) unit 1, (b) unit 2 and (c) unit 3 for positive x-direction winds

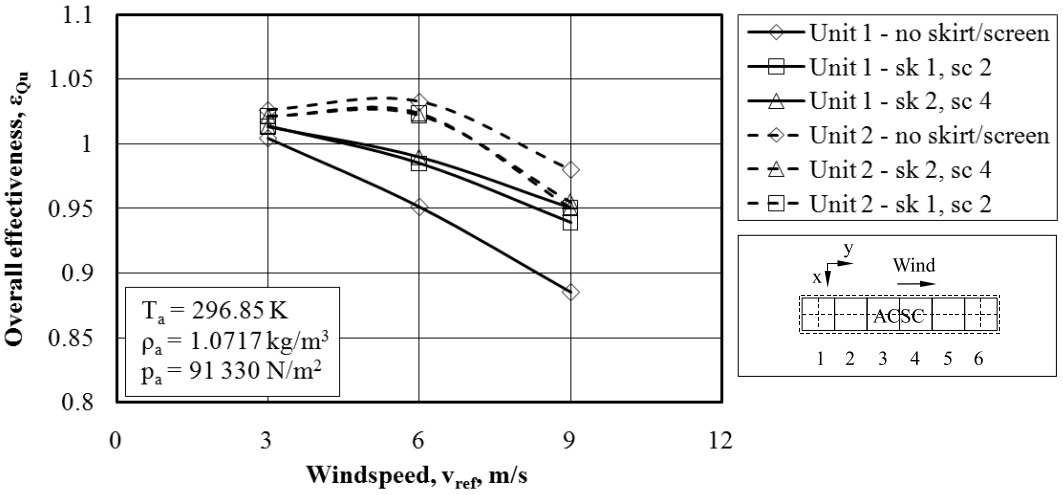

(a)

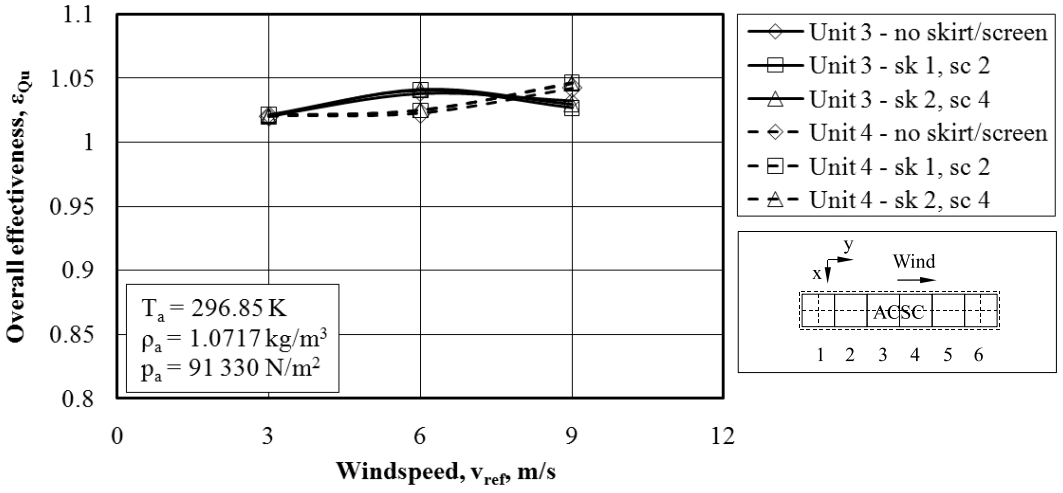

(b)

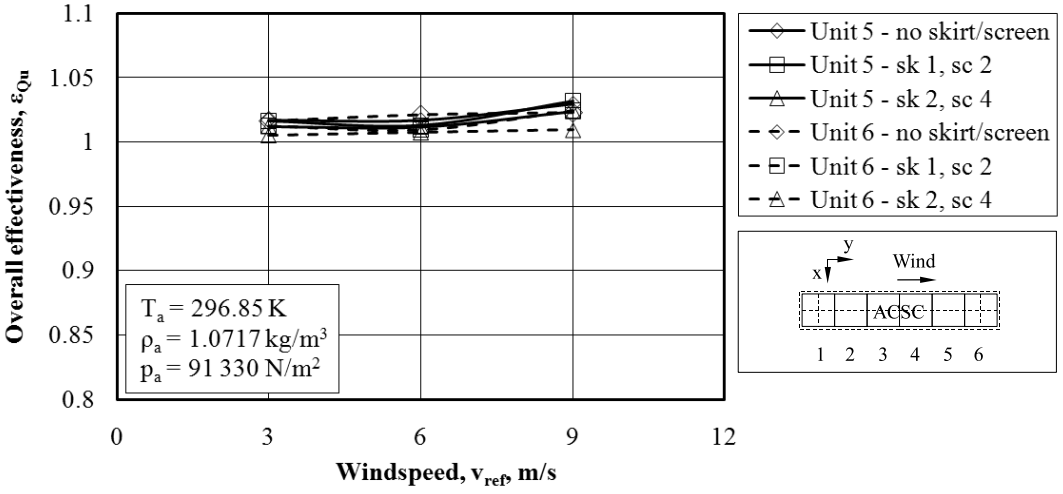

(c)

Figure F.4: The combined effect of various skirt-screen configurations on the overall effectiveness of (a) units 1 and 2, (b) units 3 and 4 and (c) units 5 and 6 for positive y-direction winds

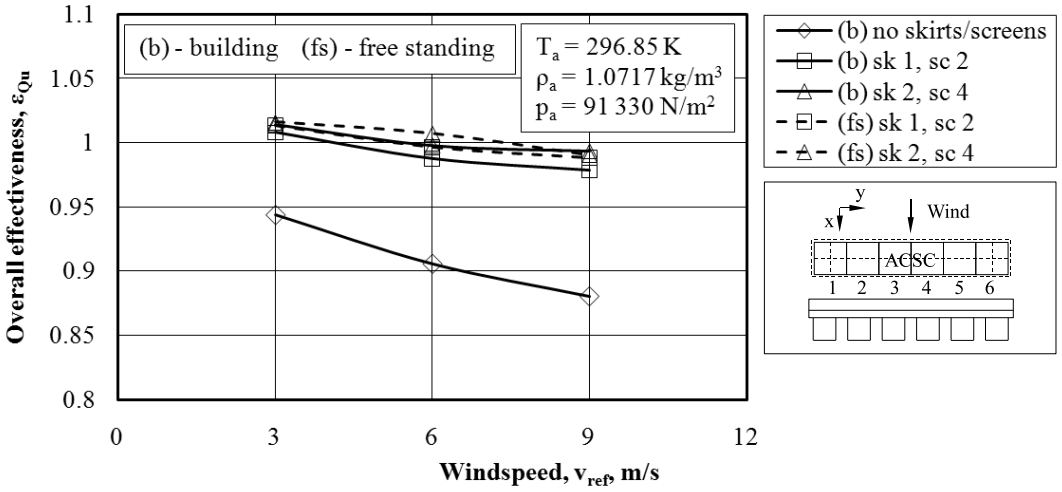

(a)

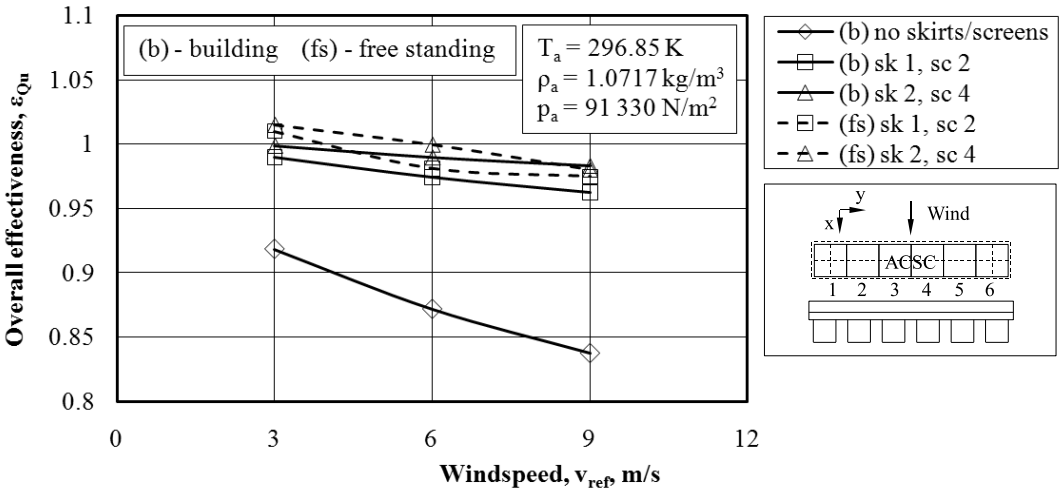

(b)

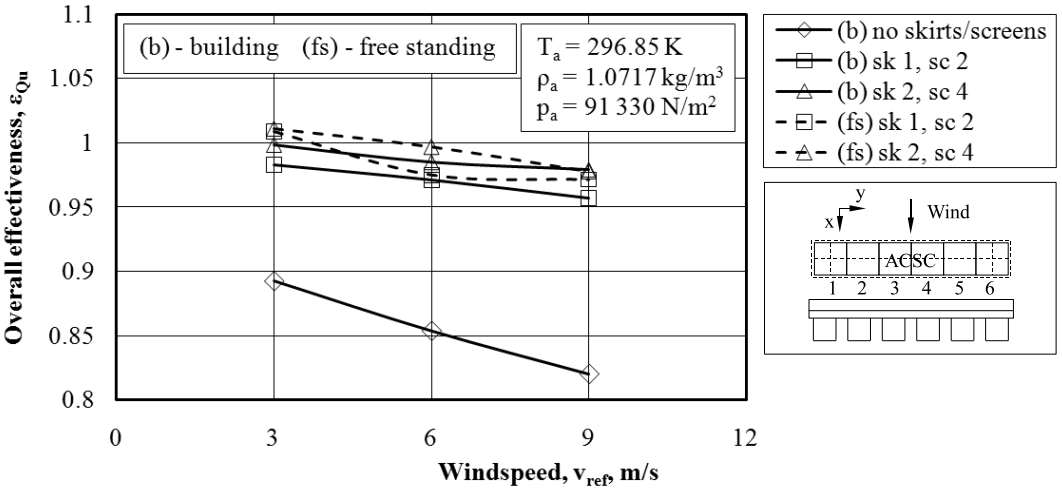

(c)

Figure F.5: The combined effect of power station building placement as well as various skirt-screen configurations on the overall effectiveness of (a) unit 1, (b) unit 2 and (c) unit 3 for positive x-direction winds

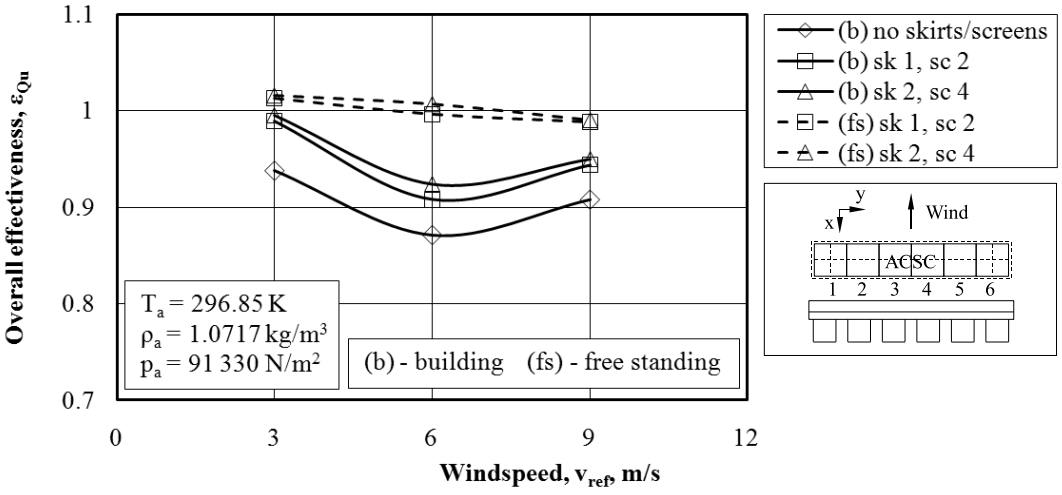

(a)

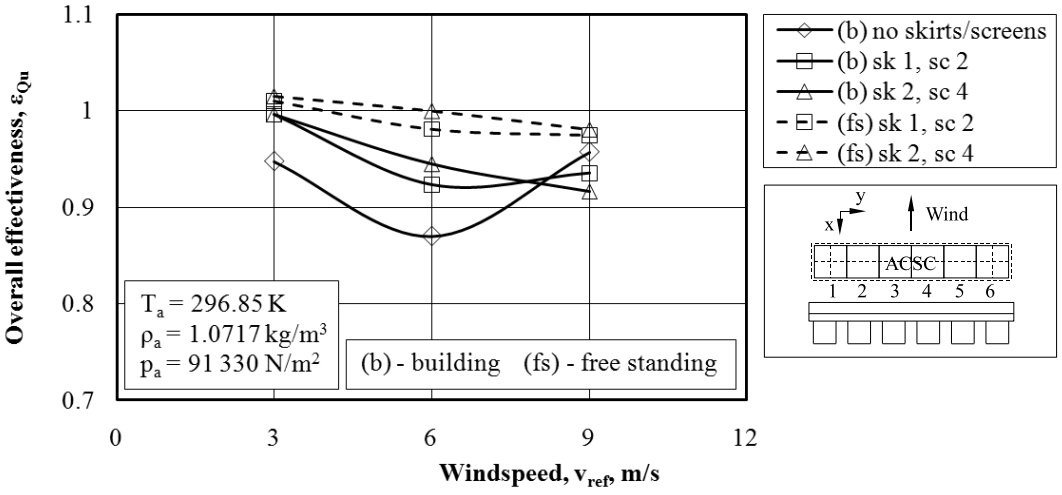

(b)

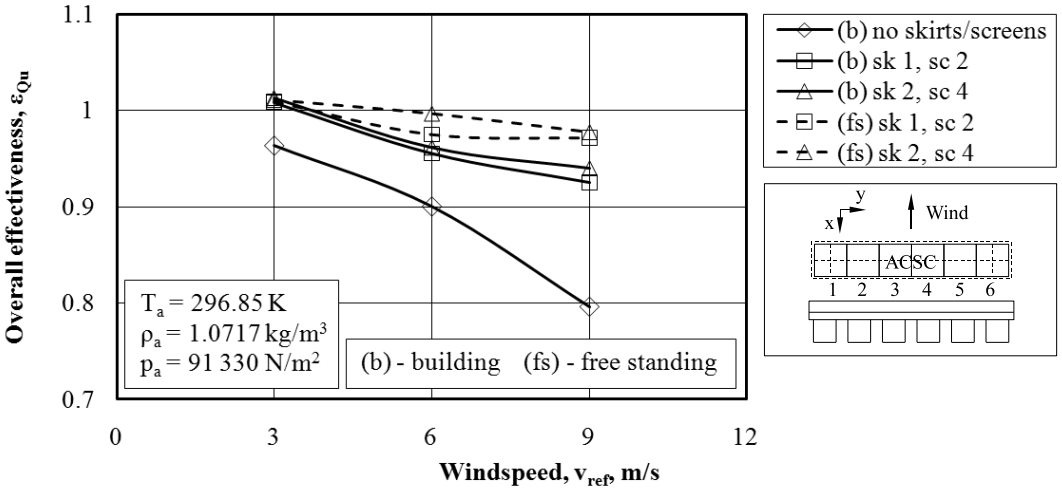

(c)

Figure F.6: The combined effect of power station building placement as well as various skirt-screen configurations on the overall effectiveness of (a) unit 1, (b) unit 2 and (c) unit 3 for negative x-direction winds